CHALMERS
UNIVERSITY OF TECHNOLOGY

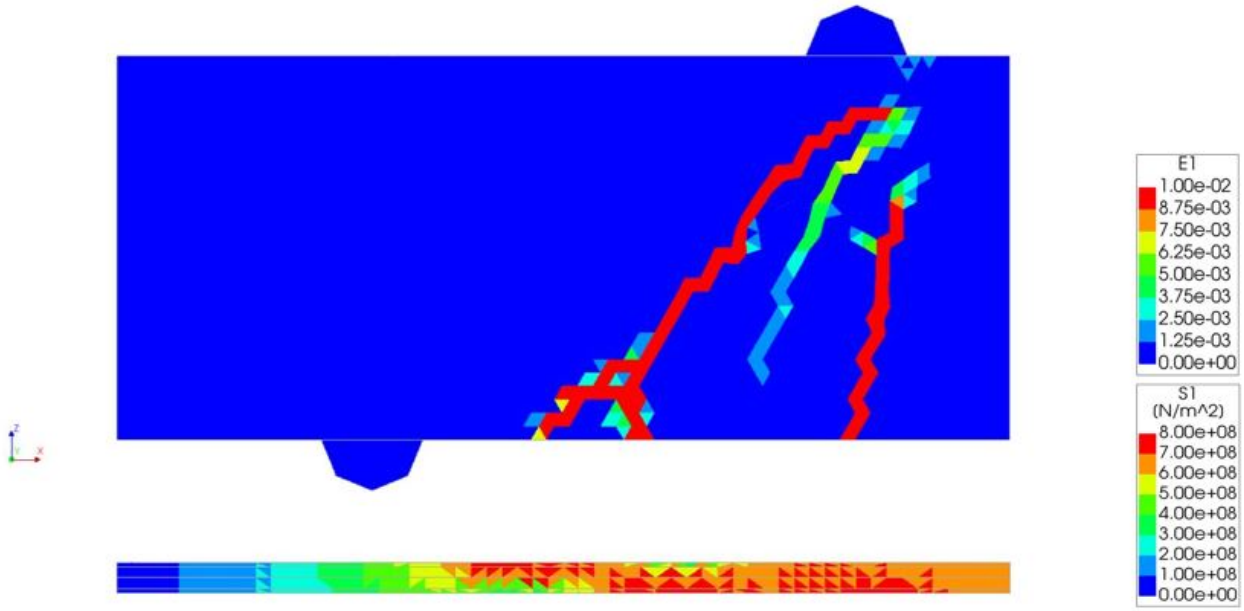

Shear Capacity of Corroded RC Structures

A study based on detailed 3D FE analyses

Master's thesis in the Master's Programme Structural Engineering and Building Technology

DAVID BERGQVIST
DAVID WALLERTZ

Department of Architecture and Civil Engineering
Division of Structural Engineering
Concrete Structures
CHALMERS UNIVERSITY OF TECHNOLOGY
Gothenburg, Sweden 2017
Master's thesis 2017:BOMX02-17-81

MASTER'S THESIS 2017:BOMX02-17-81

Shear Capacity of Corroded RC Structures

A study based on detailed 3D FE analyses

Master's thesis in the Master's Programme Structural Engineering and Building Technology

DAVID BERGQVIST
DAVID WALLERTZ

Department of Architecture and Civil Engineering
Division of Structural Engineering
Concrete Structures
CHALMERS UNIVERSITY OF TECHNOLOGY

Gothenburg, Sweden 2017

Shear Capacity of Corroded RC Structures
A study based on detailed 3D FE analyses
DAVID BERGQVIST
DAVID WALLERTZ

Master's thesis 2017:BOMX02-17-81
ISSN 1652-8557
Department of Architecture and Civil Engineering
Division of Structural Engineering
Concrete Structures
Chalmers University of Technology
SE-412 96 Gothenburg
Sweden
Telephone: +46 (0)31-772 1000

Cover:
Crack pattern with corresponding reinforcement stress for the verified FE model

Chalmers Reproservice
Gothenburg, Sweden 2017

Shear Capacity of Corroded RC Structures
A study based on detailed 3D FE analyses
Master's thesis in the Master's Programme Structural Engineering and Building Technology
DAVID BERGQVIST
DAVID WALLERTZ
Department of Architecture and Civil Engineering
Division of Structural Engineering
Concrete Structures
Chalmers University of Technology

ABSTRACT

One of the main reasons for deterioration of reinforced concrete structures is corrosion of the steel reinforcement. Knowledge regarding the behavior of corrosion damaged structures is crucial for proper structural assessments and maintenance plans. Many studies have investigated how corrosion affects the main reinforcement, mainly with the reduction of cross section and stresses induced by rust expansion, as well as cracking of the concrete cover. However, there is little research concerning how the shear behavior is affected. In particular how corrosion influences the shear crack angle, and also the influence of stirrups stresses induced by corrosion of the main reinforcement. Expanding the knowledge with regard to these aspects is the focal points of this paper as this will aid the assessment of shear capacity in corroded reinforced concrete structures.

In this Master's thesis, a detailed 3D finite element (FE) model was used to investigate the shear behavior of beams subjected to different levels of corrosion, with the focus on shear crack angle and stirrup stresses. To properly examine the behavior, the FE model includes a bond and corrosion model at the interface between concrete and reinforcement; another bond model is also used for the interaction between the steel supports and the concrete. The FE model is verified against an experimental four-point bending test in terms of ultimate capacity, stiffness, and crack pattern and a parametric study is performed to investigate the influence on the shear crack angle. The same FE model was then used to evaluate the effect of corrosion of main reinforcement on tensile stresses in neighboring stirrups.

The results indicate that corrosion affects the shear crack development. With increased corrosion, the shear cracks show a decreased angle to the horizontal, and for some cases a crack propagates along the reinforcement towards the supports. Furthermore, increasing corrosion leads to additional cracks. Finally, the results from the analyses of the stirrup stresses induced by corroded main reinforcement shows a significant effect on the shear capacity, with stress levels close to yielding.

Keywords: reinforced concrete beam, corrosion, shear angle, bond, reinforcement, stirrups

CONTENTS

PREFACE

This thesis was performed during the spring of 2017, at the Department of Civil and Environmental Engineering, Division of Structural Engineering, Concrete Structures, Chalmers University of Technology. Supervisors of the project were Mattias Blomfors, Lic. Engineer, and examiner and supervisor, Ph.D. Kamyab Zandi. The project is a part of the ongoing project ARC, Assessment of anchorage in corroded Reinforced Concrete Structures, financed by the Swedish Transport Administration (Trafikverket), SBUF and CBI's Consortium for the Financing of fundamental Concrete Research (CBI's A-konsortiet). The FE modelling in the project is performed in the software DIANA 10.1 (TNO, 2017).

We are grateful for the help and guidance our supervisors Kamyab Zandi and Mattias Blomfors have given us during the project. A big thank you is dedicated to them. We would also like to pay tribute to "Fikagruppen", our source of motivation.

Gothenburg, June 2017

David Bergqvist

David Wallertz

NOMENCLATURE

Roman upper case letters

E_c	Young's modulus of concrete
E_s	Young's modulus of steel
G_F	Fracture energy of concrete
$V_{element}$	Element volume

Roman lower case letters

f_c	Concrete compression strength
f_{cm}	Concrete mean compression strength
f_{ct}	Concrete tensile strength
f_u	Reinforcement ultimate strength
f_y	Reinforcement yield strength
h	Crack band width
k	Friction factor in bond slip model
r	Radius of bar
w_{crack}	Crack width
x	Corrosion penetration

Greek lower case letters

ϵ	Strain
ϕ	Diameter
ν	Poisson's ratio
ρ	Density
σ	Stress

1 Introduction

1.1 Background

Reinforced concrete structures represent a large part of the existing structures in our society which emphasizes the reasons to improve the understanding of the structural behaviour. These structures suffers from deterioration, where corrosion of reinforcement is the most severe reason (Bell, 2004). Even when corrosion occurs in reinforced concrete (RC), the structure may still be serviceable and thus it is of importance to assess the structural behaviour and capacity. Many researchers have treated the subject with different focal points in order to improve the assessment of deteriorated structures so that suitable actions could be performed instead of perhaps unnecessary replacement. The main effects of corrosion are the decrease of the cross-sectional area of the reinforcement together with cracking in the confining concrete due to expansion of rust. This may cause decreased bond capacity which increase the probability of anchorage failure (Lundgren, Nilsson, et al., 2014), but also may affect the ductility of the steel (Zandi Hanjari, 2010). The interaction between reinforcement and concrete is essential for the RC structures and affects the load-carrying capacity as well as the stiffness and crack distribution (Zandi Hanjari, 2010). The expansion of the reinforcement caused by corrosion may also influence the adjacent stirrups and induce tensile stresses that can reduce the shear capacity of the stirrups (Zandi, 2014b). When designing stirrups for RC structures the shear crack angle is an important factor in for example the strut-and-tie method. However, for deteriorated structures this angle may change with different corrosion levels. Therefore guidelines regarding the effect of corrosion on the angle is important to properly determine the residual shear capacity. The Master's thesis is a part of the project "Assessment of anchorage in corroded Reinforced Concrete structures, ARC", which has proven it's value in a pilot study by Nilsson and Lundgren (2014a), Nilsson and Lundgren (2014b) and Lundgren, Nilsson, et al. (2014). The ongoing project, financed by the Swedish Transport Administration(Trafikverket), SBUF and CBI's Consortium for the Financing of fundamental Concrete Research (CBI's A-konsortiet), has the aim to determine the life spans and load-carrying capacity of existing infrastructures.

1.2 Problem description

It is of interest to determine to what extent corrosion affects RC structures, and especially the behaviour of the stirrups and the shear capacity since such research is limited. When corrosion occurs in the main reinforcement of a RC structure the cross section of the reinforcement will decrease, hence a loss in tensile capacity of the reinforcement, but also cracking in the confining concrete due to the rust expansion which will lead to decreasing compressive strength. When determining the residual shear capacity, it is important to know the effect of corrosion on the shear crack angle, this constitutes the first focal point of this thesis. Furthermore the effectiveness of stirrups will be influenced by the bond and anchorage capacity of the main reinforcement due to the effect of the varying shear crack angle. Additionally, the corroding main bars will expand and thus induce stresses in stirrups which may affect the shear capacity. This matter constitutes the second focal point of the Master's thesis.

1.3 General goal

The ambition is to study how the shear crack angle varies for the corrosion related problems described above. The thesis should also describe and quantify the effect of the stresses induced to the stirrups by corroding main bars. To provide content to the thesis, the aim is to describe the practical importance of solving the problems and what gains the society can achieve.

1.4 Methods

The work includes a literature study as well as studying available shear tests on corroded and uncorroded bars to get understanding of the field. It is complemented by a study of three-dimensional (3D) non-linear finite element (NLFE) analyses in the FE software DIANA to reach the goal of the thesis and quantify the influence of corrosion. The NLFE model was validated against existing FE models and experimental tests and further developed to capture the behaviour of a corroded beam. The first focal point, regarding the shear crack angle of RC structures, have many factors that might influence the shear behaviour when corrosion occurs. Therefore a parametric study is required to properly describe the development.

1.5 Limitations

One limitation in a project including a parametric study like this is the number of parameters. Some of the parameters that were discussed but neglected were more related to the longitudinal reinforcement, as bar size and arrangement, and the stirrups arrangement and design. The stirrups were modelled as embedded elements in the FE model for simplicity and computational time reasons. The interaction between the reinforcement and the confining concrete was modelled with a bond model according to Lundgren (2005a). There are other models to describe the bond behaviour, however they were not included in the present study. The thesis is also limited to only include one cracking model, a rotating crack model. Furthermore, only one type of boundary conditions is treated, simply supported. The beam analyzed is limited to one size, except from in the parametric study where one additional shear span is studied. Size and dimension effects is therefore a limitation of this thesis. Finally, the analyses does not include the influence of long term loading, such as creep and shrinkage.

2 Theoretical background

2.1 Concrete cracking

For a reinforced concrete beam, there is three different stages in terms of the behaviour depending on the load applied. In stage I, the cross section is uncracked, the beam have a large flexural rigidity and the deformation increases linearly with the load. But as soon as the concrete tensile strength is reached for a certain load, a flexural crack will form in the section of maximum moment. At this moment, stage II initiates for this cross section while the uncracked sections remain in stage I. This event will be distinguish on the load-deflection curve since after this point the stiffness will decrease. The last stage occurs when the reinforcement reach yielding. In order for an inclined shear crack to initiate, the tensile capacity needs to be exceeded by the principal tensile stress in the shear span. For a section where the bending moment is large but the shear force is moderate, a flexural crack will develop perpendicular to the edge in tension, but if the section exhibits large shear forces, the crack will initiate the same way but then propagate in an inclined direction instead (Al-Emrani et al., 2013).

2.2 Shear capacity of concrete structures

In a section close to the support in an uncracked simply supported beam, the contribution from the flexural stresses are very small and the principal stresses is almost solely dependent on the shear stresses. The shear stresses, which is highest in the center of gravity, will give the maximum principle stresses at an angle of 45°relative to the beam direction (Al-Emrani et al., 2013). These stress relations are described by Figure 2.1.

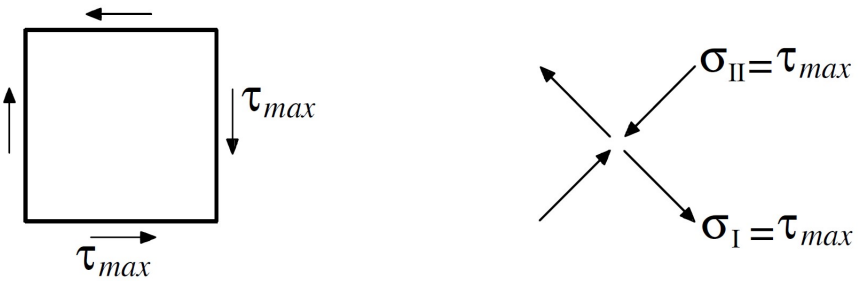

Figure 2.1: Shear stresses acting on an element in the center of gravity which result in the principle stresses σ_I and σ_{II} (Al-Emrani et al., 2013)

Web shear cracks are caused by the principal tensile stresses, often very close to the support. The nearer the mid span, the larger is the contribution of the flexural stresses and it is more likely that the shear crack will begin as a flexural crack, a so-called flexural shear crack. Although some of the shear forces can be taken by friction in the shear crack and dowel action in the longitudinal reinforcement, the stirrups are

to be designed to carry the full shear forces. The maximum spacing between the stirrups is therefore designed so that at least one stirrup crosses a possible shear crack, which normally is chosen to be inclined with the range of 22 - 45°according to Eurocode 2 (2004). When corrosion of the reinforcement is initiated, the capacity of the longitudinal and transverse reinforcement is affected differently and the stresses are redistributed, partly also because of the cracking as a result of corrosion (Al-Emrani et al., 2013). This redistribution will affect the shear crack angle and one focal point of this thesis is to quantify this variation of the angle. A lower angle increases the stresses in the longitudinal reinforcement caused by shear stresses and therefore also increases the requirement of proper anchorage (Engström, 2015).

Regarding how corrosion affects the angle of shear cracks and how this should be considered in design of RC beams, there are to the authors' knowledge not any studies made earlier in this specific field. The main focus for papers and articles concerning corrosion in beams is often on the longitudinal reinforcement; however, the problem regarding how corrosion influences the shear capacity is not treated comprehensively. Especially, stirrups stresses induced by corrosion in the main bars which is the second focal point of this thesis.

The most common shear failure mode for a reinforced structure without stirrups is a flexural shear failure (Al-Emrani et al., 2013), which is often initiated as a flexural crack that propagates to an inclined shear crack which causes the failure. For cases where the crack instead is formed as a web shear crack, the failure mode will still be similar. The capacity is based on the friction along the crack and is affected by the doweling effect from the longitudinal reinforcement which holds the crack together in the tensioned section. In order to avoid these failures, addition of stirrups to the beam could results in a delay of the shear failure until the stirrups yields. However, an increased shear capacity because of stirrups in the structure allows a higher shear force and another failure mode is possible - web shear compression failure. When designing structures including stirrups, Eurocode 2 (2004) recommends an angle between 22 and 45° relative to the beam axis for the compression strut. This is used to determine the shear capacity in a truss model.

2.2.1 Strut-and-tie method

The strut-and-tie method has been developed by Schlaich et al. (1987) and was adopted by Eurocode 2 (2004). The purpose of the method is to simulate a stress field in a reinforced concrete structure that has cracked and is in the ultimate limit state. The model is based on the theory of plasticity and the method is often used when designing deep beams and discontinuity regions. The struts carry compression while the ties carry tension. For slender members, such as beams or columns, the inclined struts can be extended in order to achieve a compatible angle between the strut and the tie. This extension is called a "truss model" and for this to be possible, closely spaced stirrups are needed to carry the shear forces by vertical ties, see Figure 2.2.

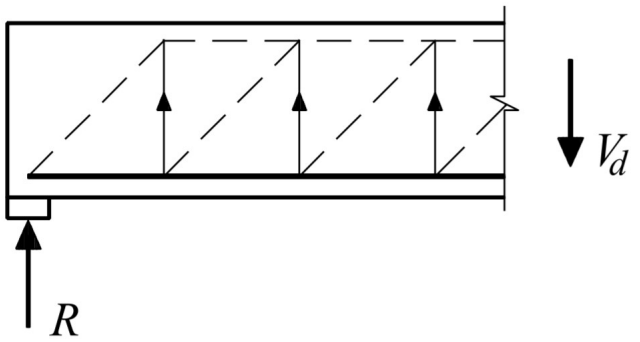

Figure 2.2: Truss model where the shear force is carried by inclined compression struts and vertical stirrups (Engström, 2015)

2.3 Effect of corrosion on concrete structures

For reinforced concrete structures, one of the most severe deterioration mechanisms is corrosion of reinforcement (Bell, 2004). The service life of concrete structures is, to a large extent, depending on the corrosion level and the resulting structural effects. When maintaining existing structures in the past, without the knowledge gained in this and accompanied projects, one part of the structure could be replaced due to corrosion even though the capacity could still be sufficient. Because of this, the development of methods to capture the effect of corrosion on the shear capacity is of great importance. As a matter of fact, a pilot study by Nilsson and Lundgren (2014a), Nilsson and Lundgren (2014b), and Lundgren, Nilsson, et al. (2014) showed the influence of increased knowledge in the assessment of the capacity of RC structures in the society. The assessment resulted in savings of approximately 27 mkr in maintenance for the two bridges that was parts of the study. Furthermore, the model was adopted by *fib-SAG7* as part of the Model Code for assessment of existing structures which is a proof of international recognition (Zandi, 2014a).

Undamaged concrete with a high pH value, above 12, protects the reinforcement bars with a protective passivating layer. The passivization may be broken by most commonly two different processes, chloride attacks and carbonation of the concrete. When either of this processes is initiated the reinforcement loses its protection and corrosion may propagate. The type of damage is dependent on whether the corrosion acts uniformly along the reinforcement or if it is local. These different phenomena are known as uniform and pitting corrosion, respectively. Experimental tests carried out by Zhang (2008) indicated that pitting corrosion was the main factor influencing the corrosion pattern in an initially stage. When cracks are developed, the uniform corrosion is rapidly affecting the pattern and then governs the behaviour in the second phase of the propagation (Zandi Hanjari, 2010). When corrosion of reinforcement in RC structures occurs, there is mainly two negative effects. Firstly, a reduction of the bar cross-section which leads to a reduction in moment and shear capacity. Secondly, a volume increase due to the expanding corrosion layer, where the formation of corrosion products causes splitting stresses that both affect the bond between concrete and the reinforcement and also increases the risk of concrete spalling (Lundgren, 2005b).

In a study by Juarez et al. (2011) it was stated that the deterioration of stirrups is more severe than the longitudinal reinforcement due to the smaller concrete cover, which can give a corrosion level as much as five times higher for the transverse reinforcement. It has also been seen that corrosion of the main reinforcement induces stresses in the stirrups which may affect the shear capacity. However, according to Zandi (2014b) the corrosion of the stirrups themselves in terms of the area reduction will most likely influence the shear capacity more than the induced stresses from corroded tensile reinforcement. These effects seems to be concentrated only to the area close to the longitudinal reinforcement and is thus dependent on factors as spacing and size of the main bars. However, this phenomena is only briefly researched and the amount of publications are limited. In a study made by Zhao et al. (2009) several experimental studies concerning shear capacity of corroded RC beams were examined and compared. One conclusion of the study was that the shear capacity generally was slightly higher for beams with little stirrup corrosion, less than 10% of sectional loss, than for uncorroded beams. Although, higher corrosion level of stirrups than 10% resulted in a gradually decreased shear capacity in all compared studies.

2.3.1 Development of assessment model for corroded reinforced concrete structures

There are many benefits to be gained by developing a reliable tool, yet simple to use in practice, to assess the deterioration of existing RC structures. Because of this, the Swedish Transport Administration financed a project for a PhD thesis at Chalmers from 2006-2010 which was followed up during 2010-2014. A simplified 1D-model for the Assessment of anchorage in corroded Reinforced Concrete structures, which is referred to as 1D-ARC, has been developed based on the bond-slip model in *fib* Model Code (1990) together with a 3D NLFE study by Lundgren, Kettil, et al. (2012). The model has been further improved during the years, including a verification with natural corrosion by Fernandez Perez et al. (2014), a validation by Zandi (2014b) for high corrosion leading to spalling of concrete, and even applied in practice for two corroded bridges (Nilsson and Lundgren, 2014a, Nilsson and Lundgren, 2014b, and Lundgren, Nilsson, et al., 2014) showing its potential. The model will in the future also include the influence of corrosion on the shear and bending capacity (Zandi, 2014a). The results of this Master's thesis will be of importance regarding the assessment of the shear crack angle of corroded beams as well as defining the influence that induced stresses from corroded longitudinal reinforcement may have on the shear capacity.

2.3.2 Natural corrosion versus artificial corrosion

Most available literature in the field is based on artificial corrosion. However, the experimental studies made by Lundgren, Tahershamsi, et al. (2014) uses naturally corroded specimen from an existing structure, the Stallbacka bridge. Khan et al. (2013) also studied the effect of corrosion where specimens instead were stored in an chloride environment for 19 years to simulate similar actions. Other studies in this field uses artificial corrosion. However, it could be questioned whether the accelerated corrosion rate truly represent a realistic behaviour for example according to Lundgren, Tahershamsi, et al. (2014). A high artificial corrosion rate, as in the studies by Xu and Niu (2004) (where the current density is 800 $\mu A/cm^2$) and Higgins and Farrow (2006) (600 $\mu A/cm^2$), is a factor of uncertainty. A lower rate

can be considered to have a more realistic behaviour as the studies by Zhao (2002), J. Chen (2002), and Rodriguez et al. (1997) suggest.

2.4 Bond and anchorage capacity

Corrosion of the main reinforcement also increases the probability of anchorage failures due to decreased bond capacity. Results of a decrease in anchorage capacity of about 10% was presented by Lundgren, Tahershamsi, et al. (2014) when a specimen, with up to 3% corrosion in steel mass, was compared to an uncorroded specimen. Although, another study by Lundgren (2007) shows that a low degree of corrosion does not affect the bond significantly as long as the concrete cover is uncracked and the transverse reinforcement provides enough confinement which keeps the crack together. Similar results regarding load-carrying capacity for low level of corrosion are shown in a study by Wang et al. (2010). This article indicated a reduced ductility for beams with corrosion levels under 10%. However, Lundgren (2007) states that the most severe effect of corrosion is the volume increase of the reinforcement which reduces the bond between the materials. Other papers also includes the effect of reduced ductility in the reinforcement due to corrosion which is caused by the transformation process where steel oxidizes into rust, for a state-of-art see fib (2000). A ductility reduction reduces both the moment and shear capacity as well as the stiffness. Cairns et al. (2005) states that the loss of ductility in terms of ultimate strain is the major effect of corrosion regarding the mechanical properties. Palsson and Mirza (2002) showed that a beam subjected to localized corrosion of as much as 50% of its section has entirely lost the ductility and instead acts very brittle. According to Y. G. Du et al. (2005) the decreased ductility is partly caused by the non-uniform bar cross-sectional area which the corrosion results in. A loss of bond capacity may influence the way the beam acts in regard to the shear angle, for a low bond strength the beam functions as an arch with no shear cracking (Regan and Kennedy-Reid, 2009). However, for a high bond strength the failure was caused by shear cracking and the loads could be rather well calculated by regular methods. The resistance against inclined cracking can be decreased, probably due to the increased crack widths of the flexural cracks, if the bond strength is reduced. Further, it is unlikely to obtain flexural shear cracking in the beam if the residual bond strength is very low, according to Regan and Kennedy-Reid (2009).

2.4.1 Models to describe bond and corrosion in FE analyses

There are several models to use in FE programs to describe the bond action between concrete and reinforcement. In this thesis, the bond model from Lundgren (2005a) is used and also the follow-up corrosion model form Lundgren (2005b). The bond model is calibrated on pull-out tests and the tangential strains they results in, both regard to monotonic and cyclic loading.

Bond model

The bond model used to describe the mechanism was developed by Lundgren and Gylltoft (2000) and further improved by Lundgren (2005a). The interaction between concrete and reinforcement is described

by a Coloumb friction model. The stresses are limited by two yield functions, where the first one is connected to friction and adhesion and the second to the upper limit of pull out failure. The model includes both the bond and splitting stresses which is a significant feature. The effect of the complex behaviour around a reinforcement bar, including crushing and cracking of the concrete, is included in the model as a decrease of confinement and therefore also the friction between the materials.

In the development of the original bond model the stiffness matrix was modified in Lundgren (2005a) and changed to a symmetric one. With the former asymmetric matrix, a longitudinal movement, i.e. a slip, resulted in a normal stress while the bond stress was not affected by a deformation in the normal direction. This unevenness could in some cases generate energy which is unwanted and is solved by implementing the symmetrical matrix. The modified stiffness matrix was then expanded for three-dimensional modelling with a rotational stiffness (Lundgren, 2005a). In Lundgren and Gylltoft (2000), it is described how varying bond-slip in both directions is taken into account. When slip between concrete and reinforcement occurs, the confining concrete gets crushed and the friction in the slip range loses capacity. This slip range creates a damaged zone with lower friction between the bar and the concrete. For further slip the friction will increase again and eventually create a new damage zone. Interface elements are placed in the FE software between the concrete and the reinforcement and represents the relationship between stresses and displacements in the layer (Lundgren and Gylltoft, 2000). In Lundgren (2005a) the author describes the five parameters that are needed for the model in a two-dimensional geometry.

Corrosion model

There are mainly two effects that corrosion have on reinforced concrete structures. Apart from reduction related to loss of effective cross-section, the rust produced in this process occupies a larger area than the virgin steel, which induce stresses in the confining concrete and may cause cracking. The cracking itself affects the load-carrying capacity of a beam in different ways, partly due to spalling that decreases the internal lever arm if it occurs on the compression side, and partly due to loss of bond capacity between the reinforcement and the concrete. Because of these combined influences a combined bond and corrosion model is needed for the interface between the concrete and the reinforcement. Theoretically this model can be imagined as two separate layers but to reduce the amount of nodes for the FE-analysis they are combined into one interface Lundgren (2005b). The influence of corrosion on the friction between the materials is described in the model by a factor depending on the corrosion penetration, x, see Figure 2.3. It can be noted that the friction is increased initially due to the additional confinement for lower level of rust. This increment is however soon diminished and instead rapidly decreased, as expected when the corrosion continues.

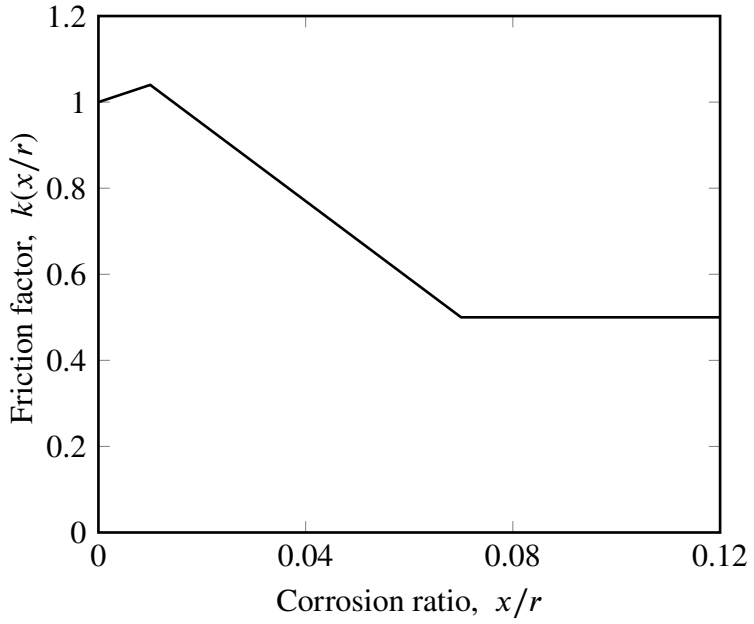

Figure 2.3: Friction model according to Lundgren (2005b)

Lundgren (2002) described how the volume increase of reinforcement due to corrosion could be handled, depending on the volume of the rust in comparison to the uncorroded steel and the corrosion penetration, where the latter were depending on time. Furthermore, Lundgren used existing experimental results of corrosion cracking tests combined with a FE study to achieve a stress versus strain diagram describing the mechanical behaviour of rust. For the rust, the strain could be determined by the deformation of the corrosion layer. These effects was neglected in Lundgren (2002) but were shown to have a slight influence on the strain in the rust in Lundgren (2005b) and were therefore included. With increasing stresses the stiffness of the rust also increases, showing a granular material behaviour of the corrosion products. There is two different approaches to describe the stress versus strain diagram in the rust. Petre-Lazar (2000) proposed that the rust initially fills the pores in the concrete close to the reinforcement which means that no stresses is induced in this phase. The other approach by Lundgren (2005b) suggests that the stresses from the increased area due to corrosion is imposed already in the beginning. When comparing the different diagrams, the first proposal shows more scatter. To complete the bond model presented by Lundgren (2005a), the friction was assumed to be affected by the corrosion which differed from the model suggested by Lundgren (2002) that neglected this impact.

2.5 Experimental results of corrosion effect on shear capacity

To be able to validate the developed 3D NLFE-model, it is compared to the one made by Taherhamsi et al. (2016) based on experimental results from Stallbacka bridge presented in the two articles Lundgren, Tahershamsi, et al. (2014) and Tahershamsi et al. (2014). The number of available experiments in this field is limited, in particular those with natural corroded reinforcement, for this reason the study mentioned fits the purpose of validation well.

The test specimens from Lundgren, Tahershamsi, et al. (2014) were obtained from the Stallbacka bridge located outside of Trollhättan in Sweden spanning 1 392 m across the Göta river. Due to poor design choices, the edge beams carried more load than designed for. This resulted in large cracks, which further lead to severe corrosion attacks. During 2010 and 2012 the bridge was extensively repaired and the edge beams were replaced. Thirteen specimens were obtained from the edge beams and divided into different corrosion levels, from no visible cracks referred to as the reference (R) to highly (H) deteriorated specimens with cover spalling. In between these levels a category denoted as medium (M), with specimens with spalling cracks, was also used. To evaluate the anchorage capacity a indirectly supported four-point-bending test was used.

Four different test setups with different pros and cons were considered for the beam test to reach an anchorage failure. Four-point bending test with indirectly supports was chosen as the best alternative, partly because some of the specimens were to damaged too be loaded with a direct support. Another reason was that the pressure from a direct support would have influenced the anchorage behaviour and provided a less accurate result. The indirect supports consisted of suspension hangers with strengthening around the supports to be able to resist the large reaction forces. The strengthening was performed by drilling vertical holes around the suspension hole and inject them with bond ribbed steel bars with epoxy adhesive. The strengthening bars, which in total were eight in number per beam, were then anchored in a steel plate on the bottom side of the beam with nuts. Since the upper reinforcement bars where more damaged by corrosion, the beams were placed upside-down so these bars would be loaded in tension. This also gave a flat upper surface for the loading points where hydraulic jacks were acting on loading plates of wood fibre and steel.

2.6 Experimental tests and FE analysis of the cracking process at shear failure

H. Du and N. Chen (2012) studied shear failure on high strength concrete based on experimental tests performed by RISE, former Sveriges Tekniska Forskningsinstitut (SP) and Betonginstitutet (CBI). The test were then compared with results from FE analyses in DIANA to analyse the factors affecting the shear capacity and the shear cracking. The test were carried out with a two-point displacement loading with a rate of 0.5 mm/min, further details regarding the setup is found in Flansbjer et al. (2011). Three different beam specimens with a w/c of 0.38 were tested to obtain the shear capacity. Throughout the loading process an optical measurement system was used to map the crack propagation at one side of the beam.

The FE investigation mainly consisted of four different types of analyses. The first one was a test to verify the tensile model to use in the FE model. Different crack models; fixed, rotating and multi-directional, were compared to mimic the behavior of the concrete in the experimental tests. With the results from the tensile test the authors decided to use a rotating crack model since it corresponded best to the compared tests in the study. The second analysis was a 2D analysis with embedded reinforcement bars and 2D plane stress elements and to more clearly describe the shear cracking a third analysis was made - a 3D analysis with tetrahedron elements. The fourth type of analysis was also a 3D analysis but with reinforcement

as solid elements and the implemented bond model from Lundgren and Gylltoft (2000) and Lundgren (2005a).

As the first object of this thesis is to determine how the shear crack angle is affected by different parameters, mainly corrosion, the work by H. Du and N. Chen (2012) fits as comparison for the uncorroded cases to validate the FE model. This because the crack propagation during the experimental tests was documented in detail. Further, the work by Du and Chen is made on a beam with simple geometry, which simplifies the parameter study in terms of time and computational requirements.

3 FE Modelling

The commercial FE software DIANA 10.1 (TNO, 2017) was used for modelling and analysis in this project. To be able to describe the bond strength and the impact of corrosion, the models developed by Lundgren (2005a) and Lundgren (2005b) were used in the FE-model. Initially the geometry from Taherhamsi et al. (2016) was used for the model which is based on the tests from Stallbacka bridge described in Lundgren, Tahershamsi, et al. (2014) and Tahershamsi et al. (2014). The results from the test and the previous FE model could give a reliable verification of the model and its input parameters. Further, the FE model was verified with simpler geometry which was later used for the parametric study in Section 3.2, to study corrosion impact on the shear crack angle. Lastly, the analysis of corrosion induced stresses in the stirrups is presented.

3.1 Verification of the bond and corrosion models

The beams from Stallbacka bridge, with dimensions and reinforcement arrangement as in Figure 3.1a, was turned up-side-down and loaded on the flat side as displayed in Figure 3.1b. In the FE model, stirrups of ϕ6 mm are placed with spacing of 300 mm in which two of them are placed in the shear span between the support and the loading plate. The stirrups are modeled as embedded reinforcement and thus not directly affected by the bond model. The support consists of a suspension hanger with an octagon-shaped hole through the beam with a diameter of 62 mm. The cross-section around the hole is reinforced by vertical embedded steel bars with ϕ16 mm.

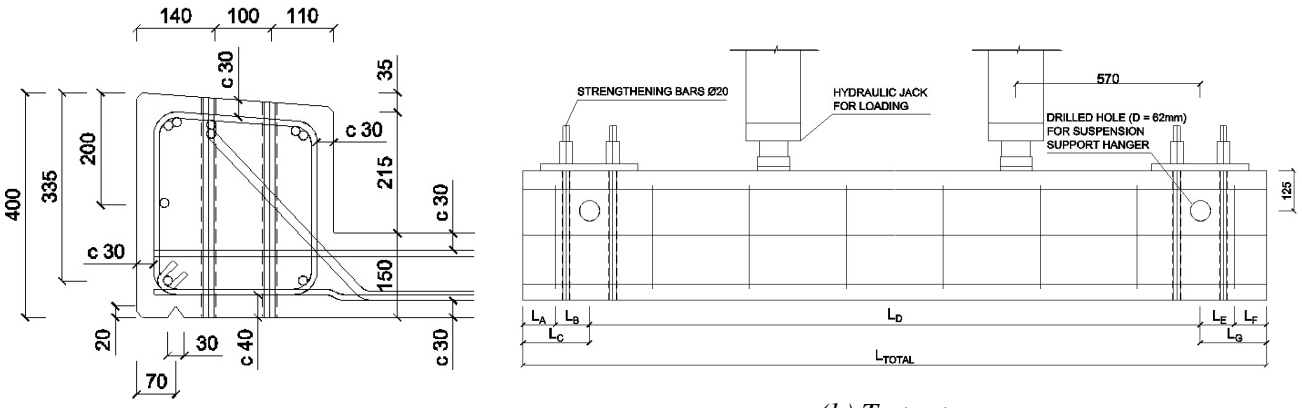

(a) Beam cross-section

(b) Test set-up

Figure 3.1: Cross-section and test set-up for the experiment of the beam from Stallbacka bridge (Tahershamsi et al., 2014)

Solid 3D elements were used to model concrete and the main reinforcement while the stirrups were modelled as embedded reinforcement elements. The geometry and input parameters such as material strengths were similar to Taherhamsi et al. (2016) and the model was used as verification for the bond- and corrosion model. The reinforcement arrangement consists of totally seven ϕ16 mm bars; two pairs of bundled bars in the bottom, one bar close to one of the sides and two bars on the top of the beam.

3.1.1 Comparative study of the beams from Stallbacka bridge

The analyses are the same as for the experiment - a four-point bending test with deformation controlled loading. Loading of the beam is made in steps of 0.1 mm up to failure. Three FE analyses are made with different tensile strengths of the concrete. According to Taherhamsi et al. (2016) the compared specimens had been damaged by micro-cracks, that could be caused by frost, which locally can mean a lower tensile capacity than that obtained from a compression test of drilled out concrete cores. Three things were analysed; stiffness, crack pattern and ultimate load. The measured concrete properties from Tahershamsi et al. (2014) scattered a bit from test to test which led to some uncertainties of which values that should be used. Properties of the materials and FE elements are listed in Table 3.1, and parameters for the analysis in Table 3.2.

Table 3.1: Input parameters for the FE models

Concrete properties	
E_{cm}	20.0 - 24.0 GPa
ρ_c	2400 kg/m^3
f_{ck}	48.1 MPa
f_{ct}	1.5 - 2.5 MPa
G_F	90.0 N/m
ν_c	0.2
Crack orientation	Rotating
Crack band width	25 mm

Steel properties	
E_s	210 GPa
ρ_s	7800 kg/m^3
ν_s	0.3
FE elements	
Element size	25 mm
Material elements	Solid tetrahedron TE12L
Interface elements	Two-plane triangular T18IF

Table 3.2: Input parameters for the non-linear analyses

Self-weight	
Load step	1
Analysis settings	Default
Mechanical load	
Load increment	0.1 mm
Iterative method	Newton Raphson
Maximum number of iterations	100
Convergence norm	Displacement
Convergence tolerance	0.01
Abort criterion	10 000
If no convergence	Terminate

Load-deflection curves with different tensile strengths were evaluated graphically in Figure 3.2 and compared with the results described in Tahershamsi et al. (2014) for the experimental test of the beam called R4 to verify the behavior of the model. The compared material properties were based on the input parameters from Taherhamsi et al. (2016) and then updated to adapt the behaviour of the experiment. A concrete tensile strength of 2.5 MPa represented the ultimate load capacity most accurately, shown in Table 3.3, even though the stiffness of the model in the early stage was overestimated.

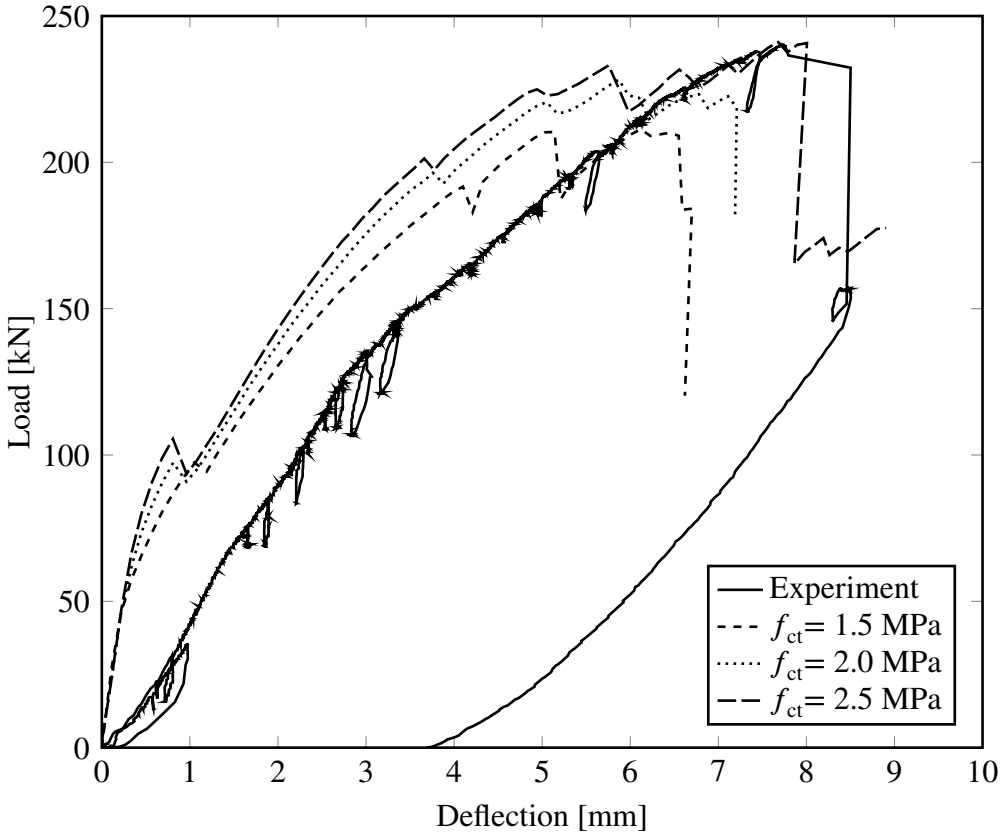

Figure 3.2: Comparison of load-deflection curves from three FE analyses with different concrete tensile strengths and the experimental tests from Tahershamsi et al. (2014)

Table 3.3: Ultimate load capacity of the reference from Tahershamsi et al. (2014) beam and the FE model with different tensile strengths

Test/model	f_{ct} [MPa]	Load [kN]
Experiment	2.8 - 3.7	240.1
FE model	1.5	211.3
FE model	2.0	228.3
FE model	2.5	241.1

The model corresponding best to experimental results in Figure 3.2 is examined further through changing the Young's modulus and the result is presented in Figure 3.3. A decreased Young's modulus results in a lower stiffness, closer to the behaviour from the experimental tests. The ultimate load capacity was nevertheless under-estimated and a lower Young's modulus was thereby disregarded.

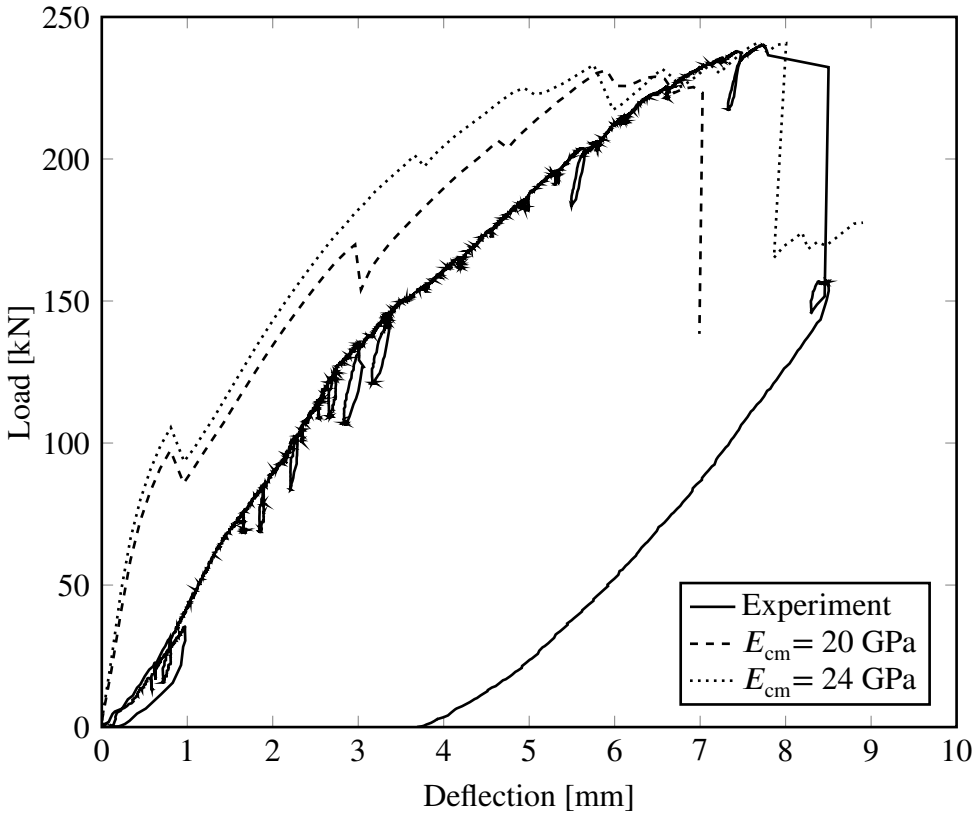

Figure 3.3: Load-deflection curves for two different values of Young's modulus compared to the experimental test of the beam from Stallbacka bridge.

Crack patterns in different load stages were analysed to see the cracking behaviour, for example the size and position of the shear cracks. These patterns were also compared to the experimental tests by Tahershamsi et al. (2014). As presented in Figure 3.4, the crack pattern from the FE analysis is similar to the experimental results, especially in regard to the localization of the first shear crack. The second shear crack is arguably initiated at the same position as in the test but propagates more vertically than in the tests, which after approaching the first shear crack turns in a more horizontal direction. The bending crack beneath the loading plate in Figure 3.4b however acts more like a flexural shear crack in the FE model. It starts as a bending crack and propagate as an inclined shear crack. Further, the shear crack from the suspension hole is initiated in the same direction in both the test and the FE model. Although, it is obvious that the experimental tests show more cracks than the FE model, this could depend on micro-cracks which is not well illustrated in the FE analysis. However, the assumption of the crack band width needs to be updated to properly describe the size of the dominating shear crack. But the main pattern is captured and especially the angle of the first shear crack which fits the purpose of the first focal point of the thesis well. This verifies the FE model and allows further exertion in the upcoming analysis.

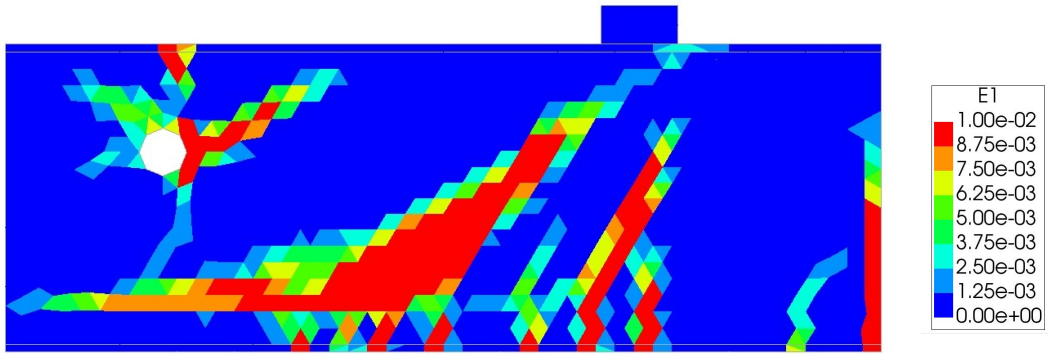

(a) FE analysis

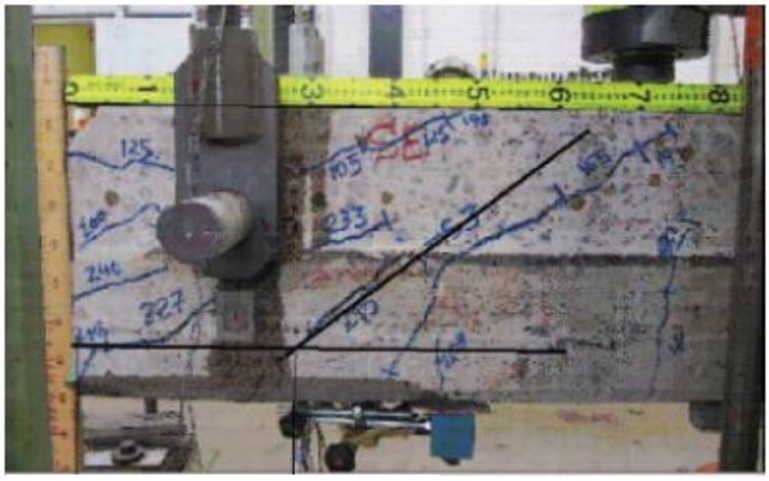

(b) Experimental test

Figure 3.4: Comparison of crack pattern between FE model in the last step of Analysis 1 and the experimental results from Tahershamsi et al. (2014).

3.2 Investigation of the shear crack angle

One of the main part of this thesis is to determine how corrosion affects the shear crack angle and the shear capacity of the RC beam. To gain further knowledge regarding the effect of different input parameters, the analyses in the investigation was carried out by shifting one parameters at the time as shown in Figure 3.5. The parametric study includes the parameters regarded as most important. Different material parameters associated with the concrete class were used, as well as different span lengths that are applied but with the height kept constant to the reference beam to get a new shear span ratio and not just a scaled beam, and finally the beam is also modelled for one case that includes stirrups according to Eurocode 2 (2004) provisions.

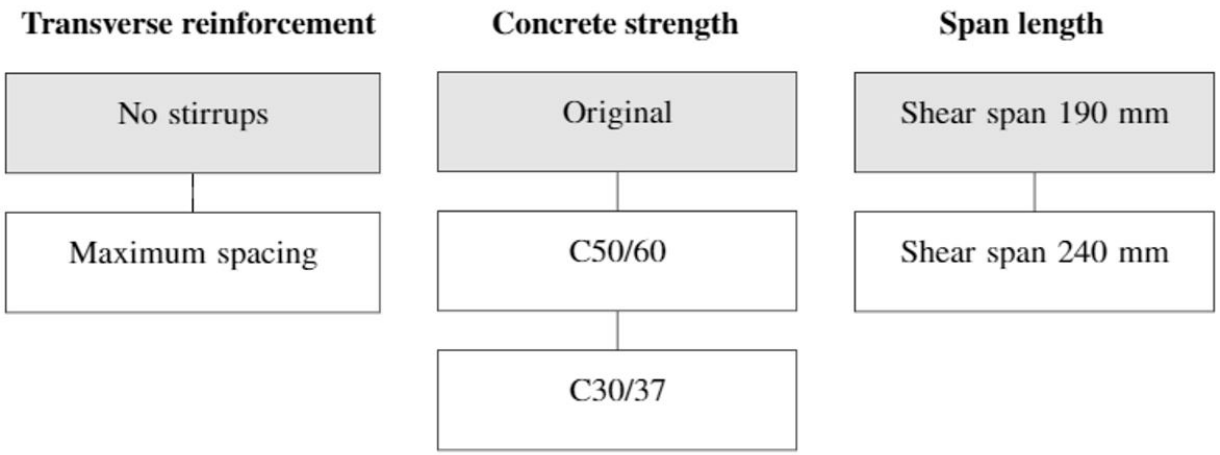

Figure 3.5: Description of the different analysis cases for the parametric study

3.2.1 Reference study and verification of the model

To make the parametric study efficient the authors decided upon using simple beam dimensions for the FE model. Since a lot of results regarding experimental shear capacity were available for tests performed by RISE and CBI, and also described in the Thesis by H. Du and N. Chen (2012), these properties were chosen as initial input parameters for the FE-model. Figure 3.6 shows the dimensions of the beam from the experiment. Although, to save modelling and analysis time, the FE model was only one quarter of the size but with corresponding boundary conditions in form of symmetry lines as displayed in Figure 3.7. The support and loading points were modelled as half octagonal prisms and the reinforcement as octagonal prisms instead of cylinders. According to Shu et al. (2015), an included bond-slip relation for the interaction between reinforcement and concrete would increase the possibility to properly describe the crack pattern in detail. Therefore, the interaction is described by a friction model. The detailed properties is showed in Appendix C, under 'MATERI', for material number 5 named 'INTERF'.

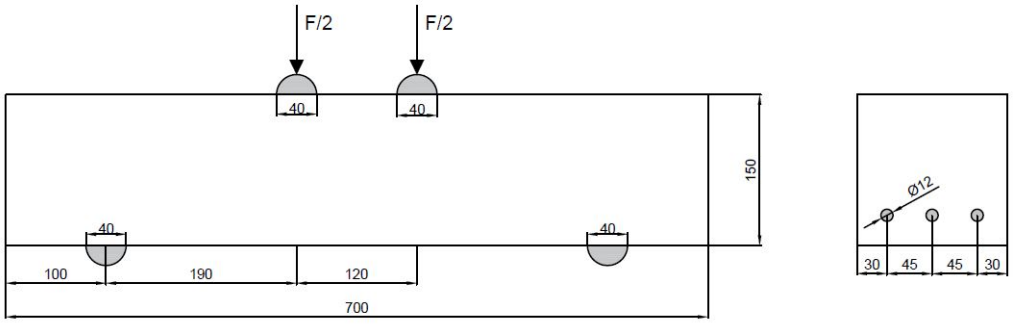

Figure 3.6: Dimensions of the beam according to H. Du and N. Chen (2012); all dimensions are in mm.

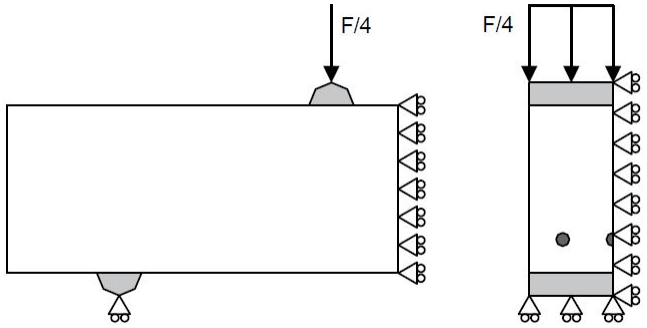

Figure 3.7: Loads and boundary conditions of the FE model.

A comparison with the experimental tests by RISE and CBI was made for the FE model for verification before the corrosion was introduced. During this iterative process many of the material and analysis parameters were updated to fit the behaviour of the experimental test better. In an early stage, different element sizes were compared. It was of importance to find a fitting element size with balance between computational time and accuracy for the parametric study to be efficient. Ultimately, an element size of

6 mm was chosen for all the following analyses.

Some of the mechanical properties such as concrete strength and Young's modulus were determined from the experiment while fracture energy and yield strength of the reinforcement had to be calibrated. A summary of these properties together with settings regarding the elements are listed in Table 3.4. The concrete compression behaviour was chosen according to Thorenfeldt et al. (1987) with a length factor of 300 mm to scale the compression curve for the element size to calibrate the behaviour (DIANA, 2017). The confinement model by Selby and Vecchio (1993) is adopted for the influence of lateral confinement on the stress-strain relation. The concrete tensile behaviour is implemented according to Hordijk (1991) with a softening curve. A hardening behaviour for the reinforcement steel was implemented similar to H. Du and N. Chen (2012), with the yield and ultimate strength defined in Table 3.4. The reinforcement stress-strain behaviour is described in Figure 3.8 for two of the compared steel qualities.

Table 3.4: Input parameters for the FE models

Concrete properties	
E_{cm}	39.5 GPa
ρ_c	2400 kg/m^3
ν_c	0.2
f_{ct}	4.9 MPa
G_F	107.0 - 208.7 N/m
f_{ck}	71.8 MPa
Crack orientation	Rotating
Crack band width	$\sqrt[3]{V_{element}}$

Steel properties	
E_s	220 GPa
ρ_s	7800 kg/m^3
ν_s	0.3
f_y	550 - 700 MPa
f_u	630 - 802 MPa
FE elements	
Element size	6 mm
Material elements	Solid tetrahedron TE12L
Interface elements	Two-plane triangular T18IF

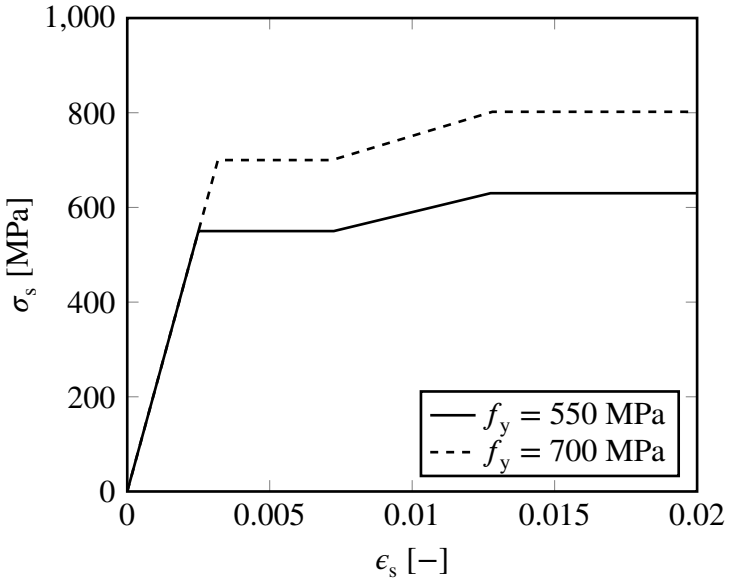

Figure 3.8: Stress-strain diagram of the reinforcement steel with implemented hardening curve for yield strength of 550 and 700 MPa.

In order to capture the post-peak behaviour of the loaded beam models, displacement controlled analyses were used. For all analyses of uncorroded beams, the iteration method by regular Newton-Raphson was used, in which the element stiffness matrix is updated for each iteration. This requires a bit more computational power but often fewer iterations than for example the Newton-modified method. Initially, the curves showed an irregular behaviour after yielding. To cope with this undesired phenomenon the convergence norm were changed to check relative energy variation instead of force and displacement. Since the interaction between the reinforcement and the concrete is modeled with a bond model, a sub-routine is required for the FE analysis to work properly. In addition, the corresponding friction model needs to be calculated depending on corrosion level according to Section 2.4.1. Further, the size of load increments is a trade off between computational requirements and accuracy of the behaviour. Different step sizes were tested and the resulting crack patterns were compared to the experiments to determine the optimal one. The decided increment size together with accompanied settings are shown in Table 3.5, it is noticed that a smaller load increment gave an undesired crack pattern.

Table 3.5: Input parameters for the non-linear analysis for the reference model

Self-weight	
Load step	1
Analysis settings	Default
Mechanical load	
Load increment	0.1 mm
Iterative method	Newton Raphson
Maximum number of iterations	400
Convergence norm	Energy
Convergence tolerance	10^{-4}
Abort criterion	10^{20}
If no convergence	Terminate

Yielding of the reinforcement was the governing parameter for the ultimate capacity and to reach the same load capacity as in the experimental test, a significantly higher steel strength was required. The yield- and ultimate strengths for all considered reinforcement qualities are listed in Table 3.6. The steel quality was updated until the capacity fitted the test which resulted in a yield strength of 700 MPa. The result of the yield strength evaluation is shown with load-deflection curves in Figure 3.9. The relation between yield and ultimate strength for the reinforcement is equal for all the different steel qualities which gives for the selected steel quality an ultimate strength of 802 MPa.

Table 3.6: Yield and ultimate strengths for the tested reinforcement steel qualities

Test/model	f_y [MPa]	f_u [MPa]	Ultimate load [kN]
Experiment	550	630	260.3
FE model	550	630	218.7
FE model	600	687	235.2
FE model	650	745	242.5
FE model	675	773	250.7
FE model	690	790	255.5
FE model	700	802	267.1

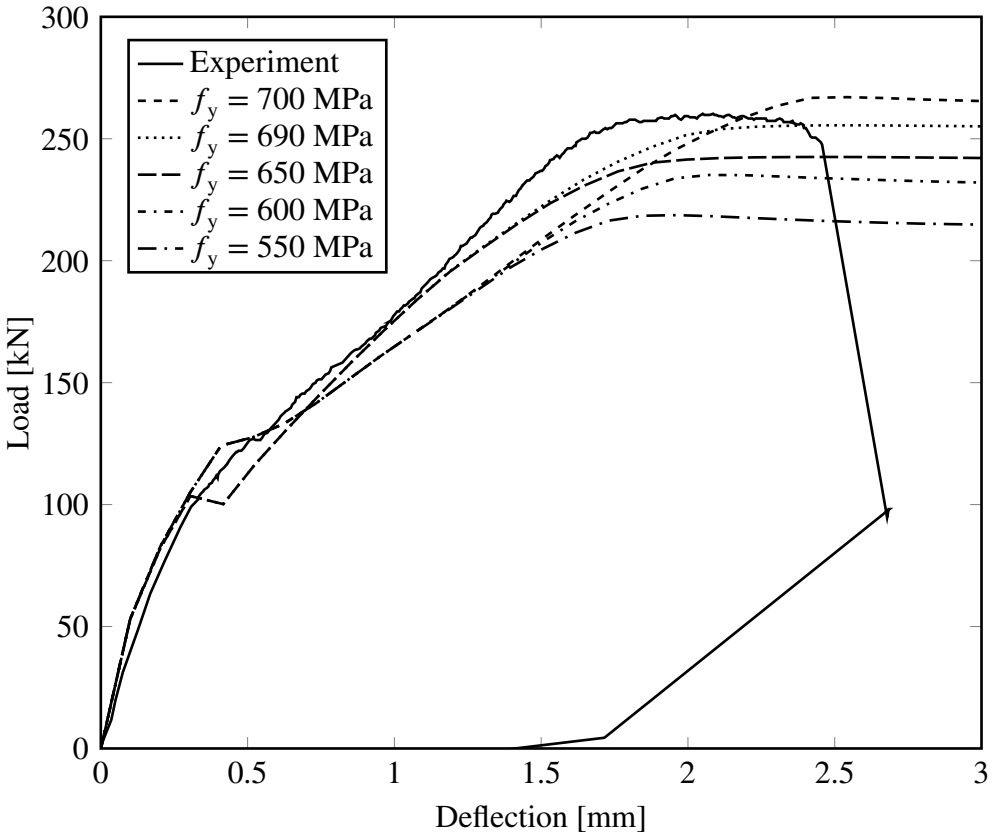

Figure 3.9: Load-deflection curves for the FE model with different reinforcement yield strengths compared to the experimental values.

After calibrating the ultimate load capacity, the beam stiffness and crack pattern was the remaining properties to calibrate. The fracture energy had a large influence on both of these properties and could therefore be refined to get closer to the actual behaviour. Three values were compared; from a direct tensile test by RISE and CBI which was described by H. Du and N. Chen (2012) - 208.7 N/m - and the ones according to Equation 3.1 from *fib* Model Code (2010) - 160.6 N/m - and Equation 3.2 from *fib* Model Code (1990) - 107.0 N/m. The equations are based on the same concrete compressive strength, which was measured in connection to the test by RISE and CBI. The evaluation was based on both the load-deflection diagram in Figure 3.10 and the crack patterns in Figure 3.11.

$$G_{\mathrm{F}} = 73 \cdot {f_{\mathrm{cm}}}^{0.18} \tag{3.1}$$

$$G_{\mathrm{F}} = G_{\mathrm{F0}} \left(\frac{f_{\mathrm{cm}}}{f_{\mathrm{cm0}}} \right)^{0.7} \tag{3.2}$$

Where f_{cm} is expressed in MPa, $f_{\mathrm{cm0}} = 10$ MPa, and $G_{\mathrm{F0}} = 25$ N/m is based on the chosen maximum aggregate size $d_{\mathrm{max}} = 8$ mm.

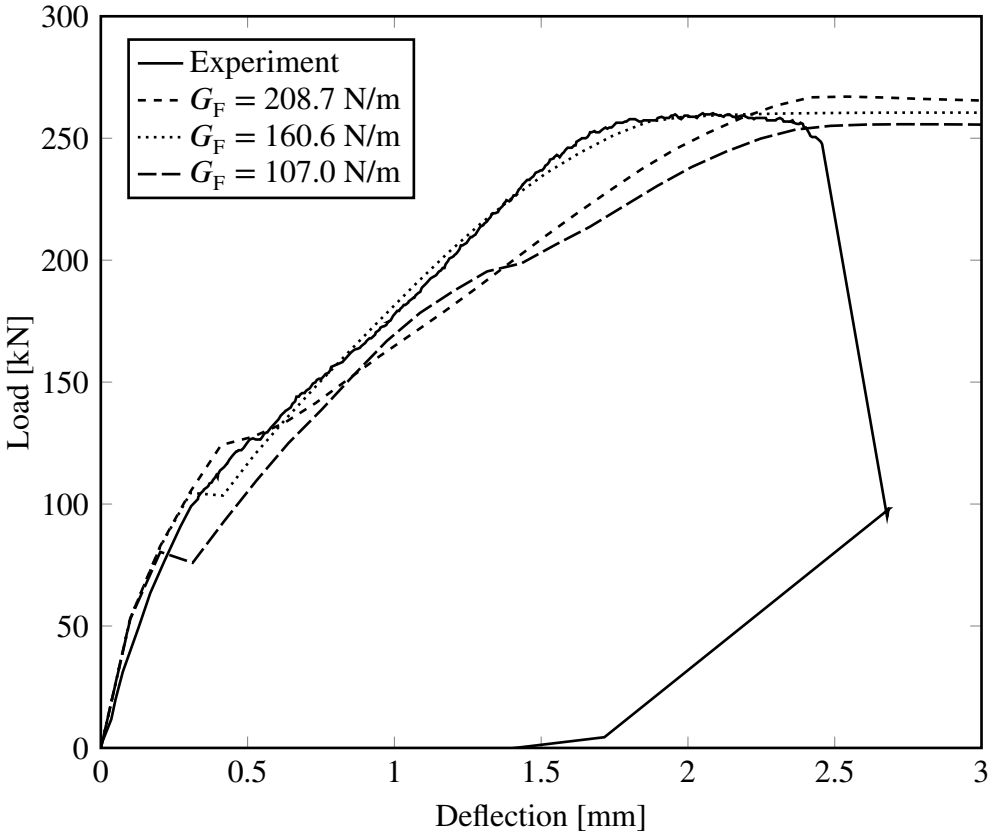

Figure 3.10: Load-deflection curves for the FE model with different concrete fracture energies compared to the experimental values.

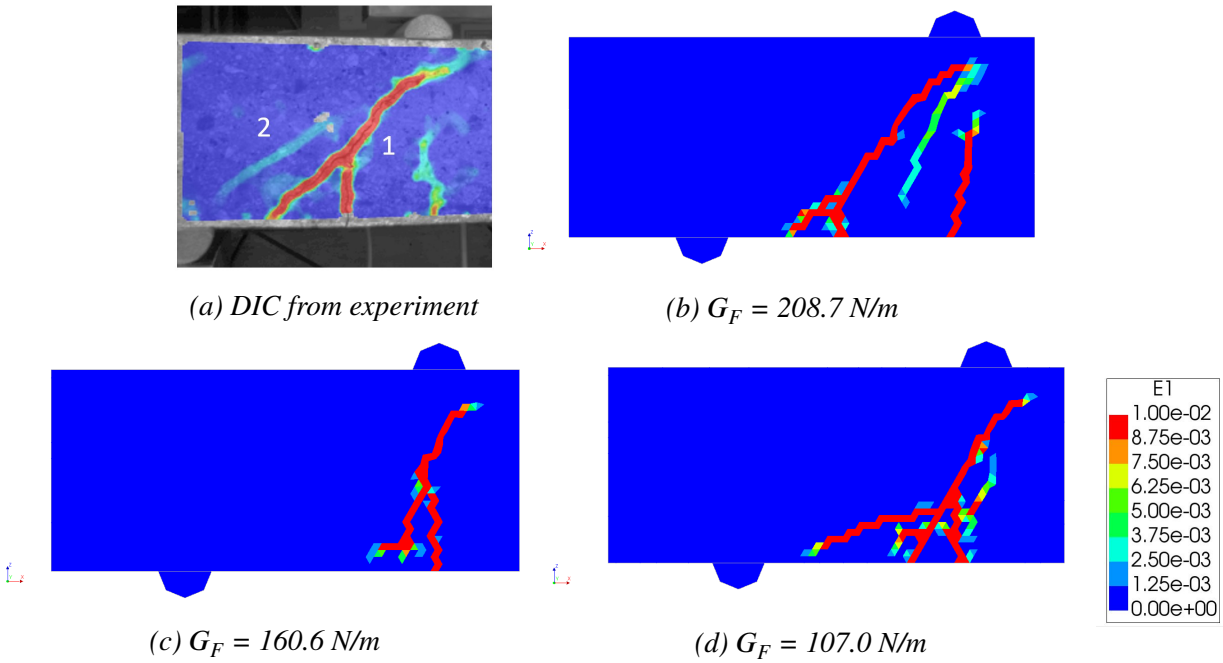

(a) DIC from experiment *(b) G_F = 208.7 N/m*

(c) G_F = 160.6 N/m *(d) G_F = 107.0 N/m*

Figure 3.11: Crack pattern for different concrete fracture energies compared with the experimental crack pattern recorded by DIC at failure load.

The model with the highest fracture energy in the comparison, the value that was determined in a direct tensile test by RISE and CBI, gave the best fit towards the experiment with regard to both the crack pattern in Figure 3.11a and the load-deflection curve in Figure 3.10. It can be mentioned that a fracture energy of 160.6 N/m gave the best fit for the stiffness of the beam but the crack pattern was not in agreement with tests. Therefore, a fracture energy of 208.7 N/m was chosen as input for further analyses. The major difference towards the experiment is the absence of the second shear crack marked with a (2) in Figure 3.11a and the propagation of the bending crack which is pronounced more in Figure 3.11b. With a stiffness and crack pattern similar to the experiment, the FE model was considered to be a good representation of the actual tests in the following corrosion analyses. This conclusion together with the previous analysis of the steel qualities resulted in the final input parameters, as listed in Table 3.7.

Table 3.7: Final input parameters for the FE models

Concrete properties	
E_{cm}	39.5 GPa
ρ_c	2400 kg/m^3
ν_c	0.2
f_{ct}	4.9 MPa
G_F	208.7 N/m
f_{ck}	71.8 MPa
Crack orientation	Rotating
Crack band width	$\sqrt[3]{V_{element}}$

Steel properties	
E_s	220 GPa
ρ_s	7800 kg/m^3
ν_s	0.3
f_y	700 MPa
f_u	802 MPa
FE elements	
Element size	6 mm
Material elements	Tetrahedron TE12L
Interface elements	Two-plane triangular T18IF

3.2.2 FE modelling of corrosion

To simulate the effect of corrosion, the model by Lundgren (2005b) was applied at the bond layer between reinforcement and concrete in the FE model. This method is described more in detail in Section 2.4.1. This part of the study is important to determine which different corrosion levels that are interesting to examine for the different cases in the parametric study. In the FE analysis, corrosion was implemented as time steps corresponding to the level of corrosion with an increment of 1 μm/s, where each second is represented by one time step. The iteration method and the other analysis choices are shown in Table 3.8. After the chosen amount of corrosion was applied, the self-weight and mechanical load steps are imposed. In order to cope with the fact that the mechanical loading is applied as a negative translation displacement in z-direction, different boundary conditions are necessary for the different load phases; corrosion, self weight and mechanical loading. This is introduced to the FE analysis by using phases where the first two are identical to the boundary conditions in Figure 3.7, while the mechanical loading phase also includes a boundary condition in z-direction for the nodes where the load is applied.

Table 3.8: Input parameters for the non-linear analysis, corrosion phase

Corrosion	
Time dependent increment	1 μm/s
Iterative method	Newton Raphson
Maximum number of iterations	100
Convergence norm (tolerance)	Energy (10^{-4})
	Force (10^{-2})
	Displacement (10^{-2})
Abort criterion	10^{20}
If no convergence	Continue

For high levels of corrosion it was difficult to obtain convergence for the mechanical load steps. The analyses required more iterations and also an even higher abort criterion to be able to continue the iterations without divergence. Other settings such as iteration method and convergence norm were kept from the previous analysis according to Table 3.9.

Table 3.9: Input parameters for the non-linear analysis, mechanical phase

Self-weight	
Load step	1
Analysis settings	Default
Mechanical load	
Load increment	0.1 mm
Iterative method	Newton Raphson
Maximum number of iterations	1000
Convergence norm	Energy
Convergence tolerance	10^{-4}
Abort criterion	10^{40}
If no convergence	Terminate

The initial corrosion study was carried out for several corrosion levels up to 55 μm (1.82% weight loss). For higher corrosion levels, the beam was unable to carry any mechanical load after the corrosion had been applied and could therefore not give any indications of the shear crack behaviour. Figure 3.12 shows load-deflection curves for four of the analysed corrosion levels.

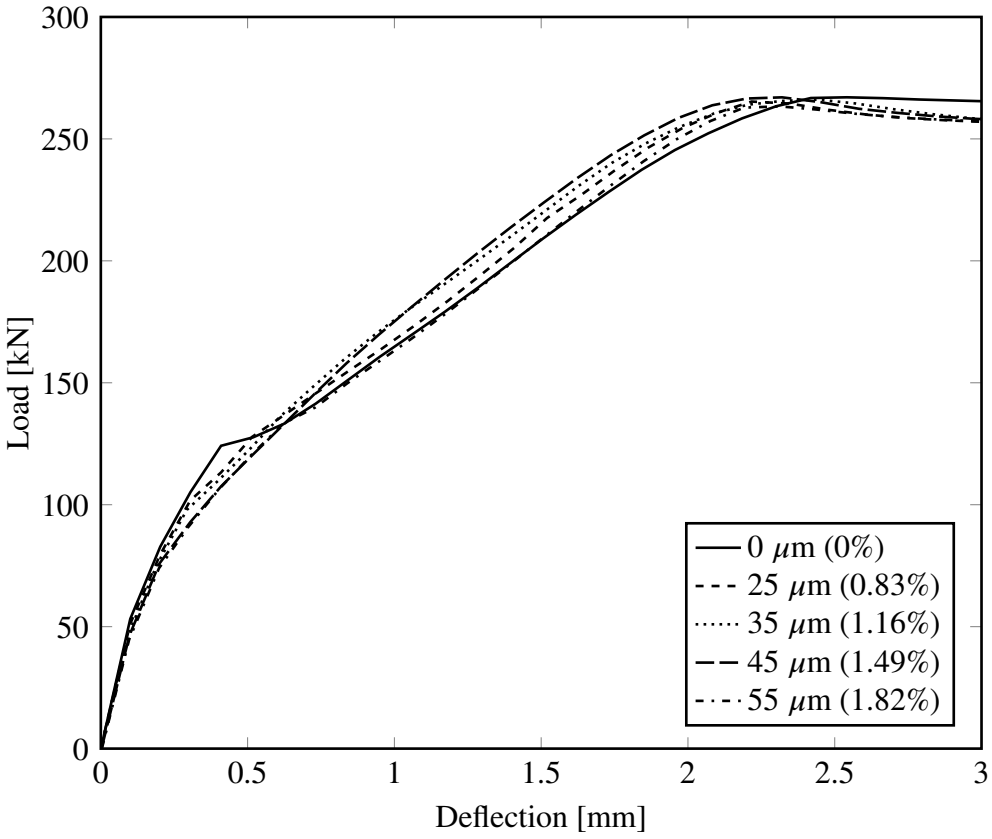

Figure 3.12: Load-deflection curves for different corrosion levels.

The ultimate load capacity for these corrosion levels was almost unaffected and the stiffness did not change significantly. However, the reduction of the bar diameter due to corrosion was not included in the bond model applied for the FE analyses and thus it was not expected to see a difference in the ultimate load levels. For the further analyses it was decided to only keep two corrosion levels in addition to the uncorroded case. The highest possible corrosion level, 55 μm (1.82%) and a value in between this and the uncorroded, 25 μm (0.83%). The parametric study presented in Section 3.2 was conducted by analysing each case for these three different corrosion levels as displayed in Figure 3.13. In each analysis the main focus is to catch the crack propagation to properly understand how the shear crack angle is affected by the different parameters, in particular the corrosion.

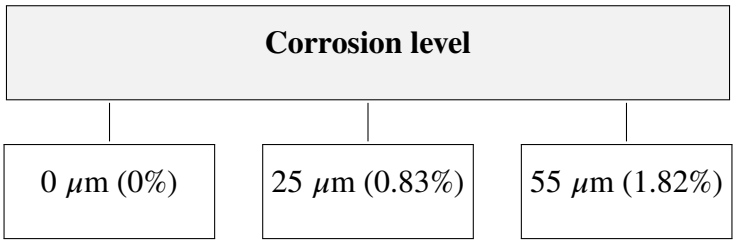

Figure 3.13: Description of the different corrosion cases for the parametric study.

For each of the three cases, the crack patterns development with the corresponding reinforcement stresses are displayed in Figure 3.14, 3.15, and 3.16 for two interesting steps in the loading process, initiation of yielding of reinforcement and at the level of the ultimate load. The figures are plotted with the first principle strain for the concrete with a contour strain of 0.01 which corresponds to a crack-width of approximately 0.05 mm, depending on the exact element size. This relation between concrete strain and crack-width is given by Equation 3.3. The plots for the corner reinforcement, which is beneath the crack pattern of the beam, show the first principle stress with positive values up to yield stress.

$$w_{\text{crack}} = \epsilon_{\text{c}} \cdot h \tag{3.3}$$

Where h is the concrete crack band width.

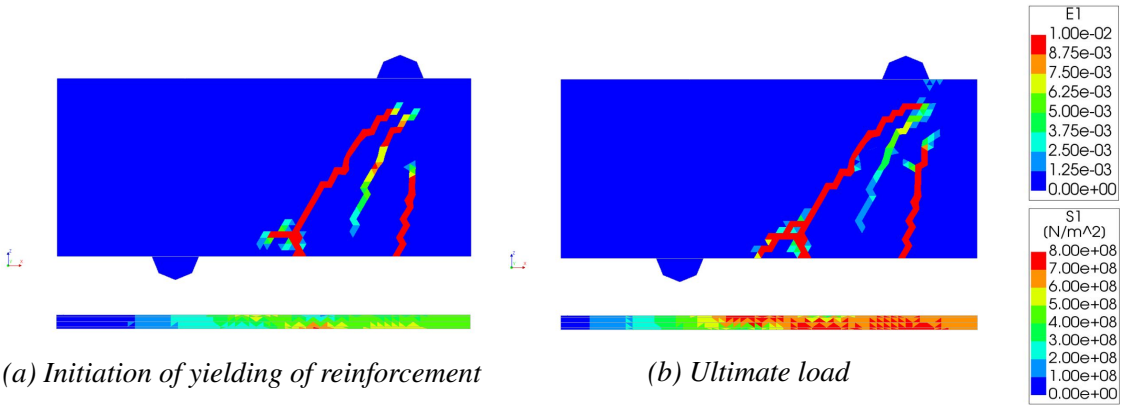

(a) Initiation of yielding of reinforcement *(b) Ultimate load*

Figure 3.14: Crack pattern and reinforcement stress for the case without corrosion.

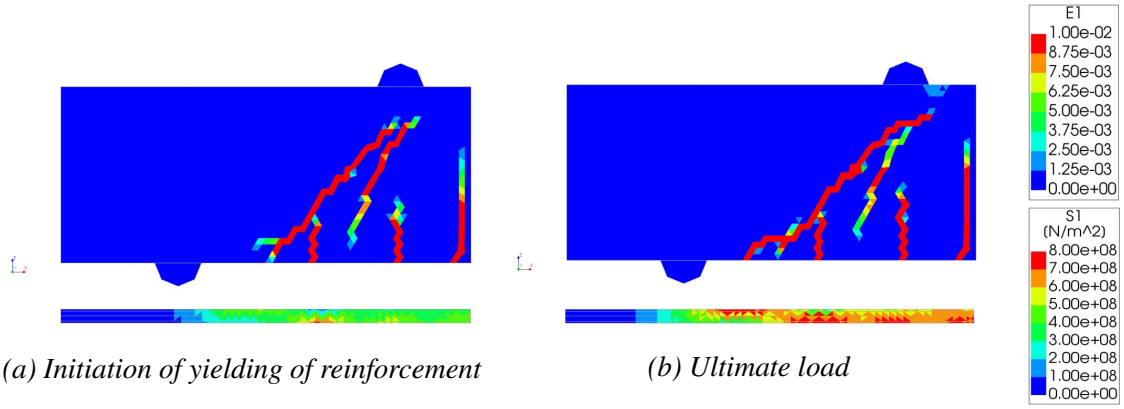

(a) Initiation of yielding of reinforcement *(b) Ultimate load*

Figure 3.15: Crack pattern and reinforcement stress for 25 µm (0.83%) corrosion.

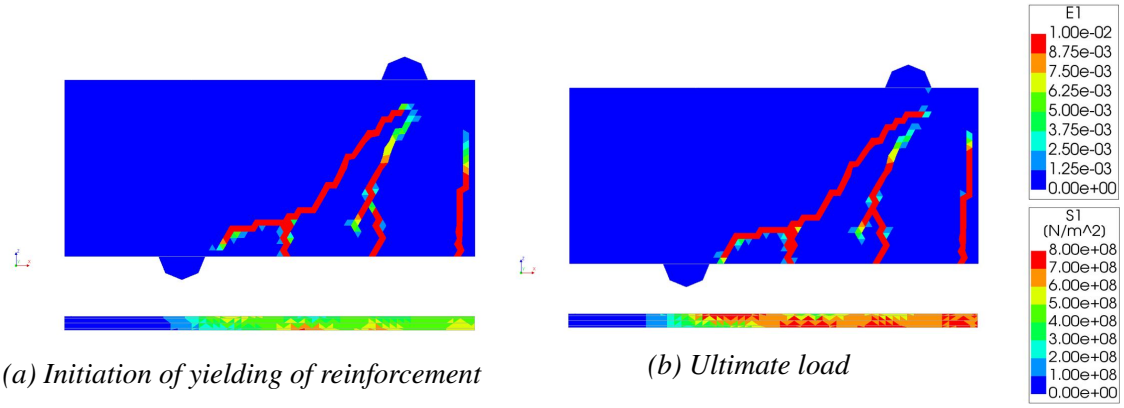

(a) Initiation of yielding of reinforcement *(b) Ultimate load*

Figure 3.16: Crack pattern and reinforcement stress for 55 µm (1.82%) corrosion.

An observation valid for all cases is that yielding is initiated where the shear crack intersect with the reinforcement. Yielding is assumed to initiate at a stage where one reinforcement element exceeds the yield limit. Another important observation is that for increasing corrosion a transverse crack along the reinforcement propagates towards the support. This shortens the available anchorage length and thereby increases the risk for anchorage failure. Furthermore, an additional bending crack emerges in the mid section while the first bending crack develops to a flexural shear crack instead. The ultimate load, i.e. the peaks of the curves in Figure 3.12, are reached when the reinforcement yields. However, the beam keeps deforming until crushing of concrete occurs. This avail at a section just to the right of the loading plate and is the final failure mode which takes place at a total beam deflection of 7-9 mm depending on the corrosion level. Even though the anchorage length for the highest corrosion level is considerably shorter, the failure mode is not changed since there is no slip. The load levels corresponding to the events displayed in the figures above are presented in Table 3.10 and Figure 3.17. Regarding the stiffness for the different corrosion levels, it is only for the uncorroded case that there is a noticeable change due to the first bending crack.

Table 3.10: Load levels for shear cracking, initiation of yielding of the reinforcement, and ultimate load

Corrosion level	Shear crack [kN]			Yielding [kN]	Ultimate load [kN]
	1^{st}	2^{nd}	3^{rd}		
No corrosion (0%)	127.6	133.3		188.9	267.1
25 μm corrosion (0.83%)	127.8	136.8	173.5	183.6	265.3
55 μm corrosion (1.82%)	106.7	139.9	198.8	198.8	263.3

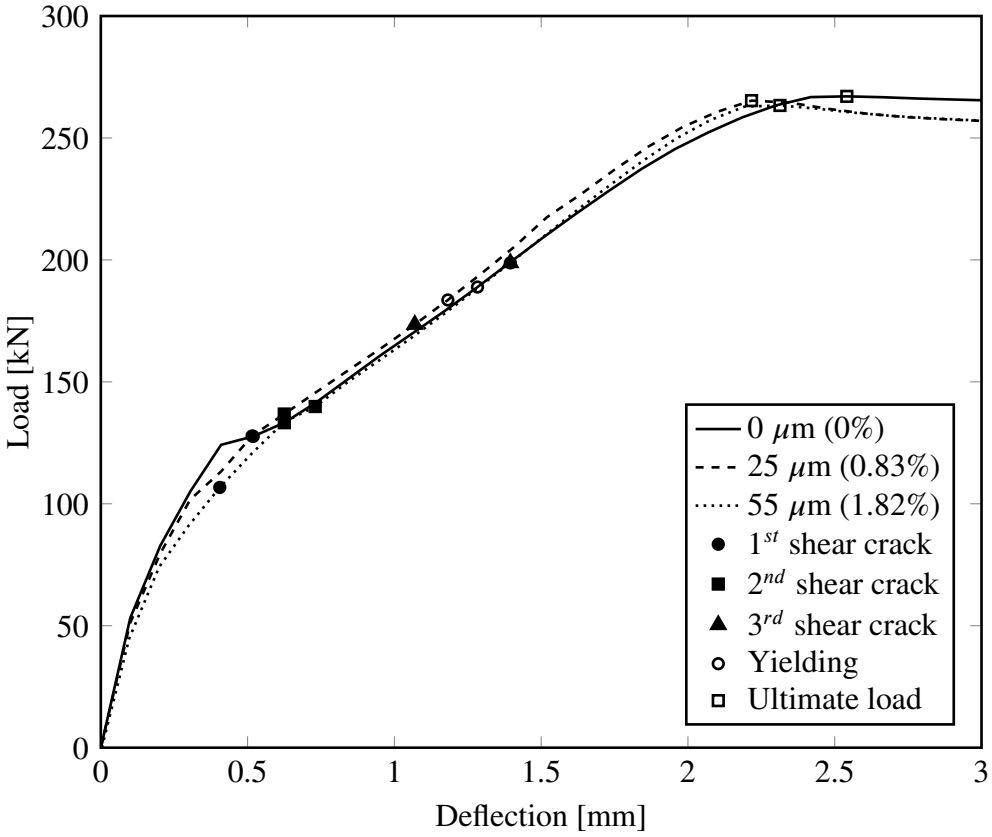

Figure 3.17: Load-deflection curves for different corrosion levels, with markers for important load levels.

3.2.3 Influence of concrete strength

In addition to the high strength concrete of the reference beam, two other concrete classes were compared in the study, with the properties listed in Table 3.11. The concrete fracture energy was computed according to *fib* Model Code (2010). The properties and analysis settings not mentioned here were the same as for the reference beam.

Table 3.11: Material input parameters for the FE models with different concrete strenghts

Concrete properties		
Class	C50/60	C30/37
E_{cm} [GPa]	37.0	33.0
f_{ck} [MPa]	50.0	30.0
f_{ct} [MPa]	4.1	2.9
G_F [N/m]	151.6	140.5
ρ_c [kg/m^3]	2400	2400
ν_c	0.2	0.2
Crack band width [mm]	$\sqrt[3]{V_{element}}$	$\sqrt[3]{V_{element}}$

Concrete class C50/60

Crack patterns and corresponding reinforcement stresses for the analyses with concrete class C50/60 are displayed in Figure 3.18, 3.19, and 3.20.

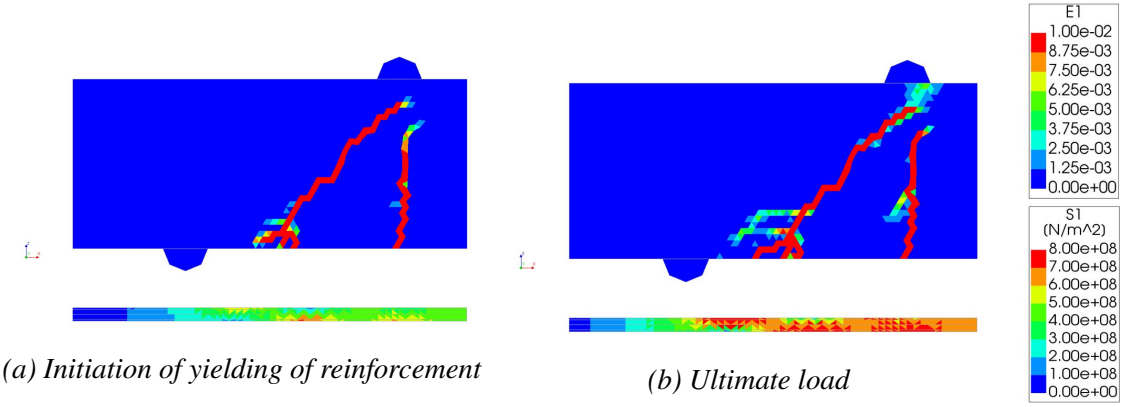

(a) Initiation of yielding of reinforcement *(b) Ultimate load*

Figure 3.18: Crack pattern for concrete class C50/60 without corrosion.

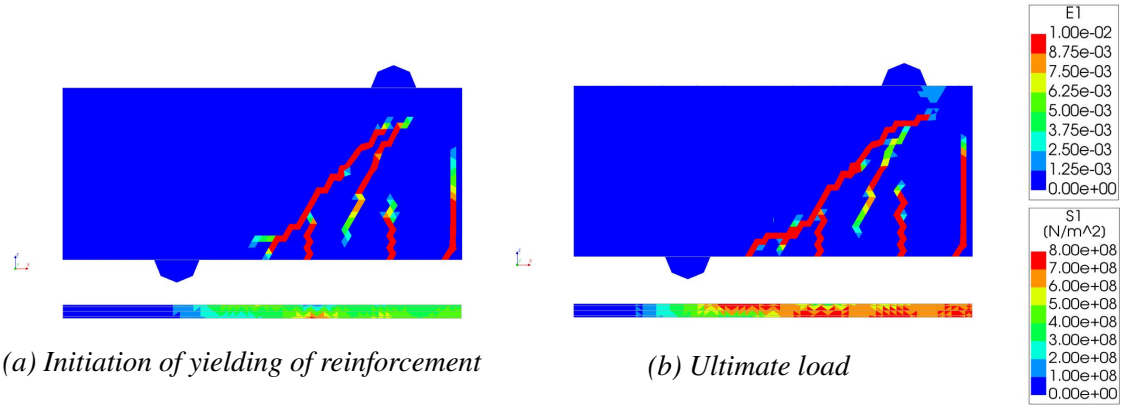

(a) Initiation of yielding of reinforcement *(b) Ultimate load*

Figure 3.19: Crack pattern for concrete class C50/60 with 25 µm (0.83%) corrosion.

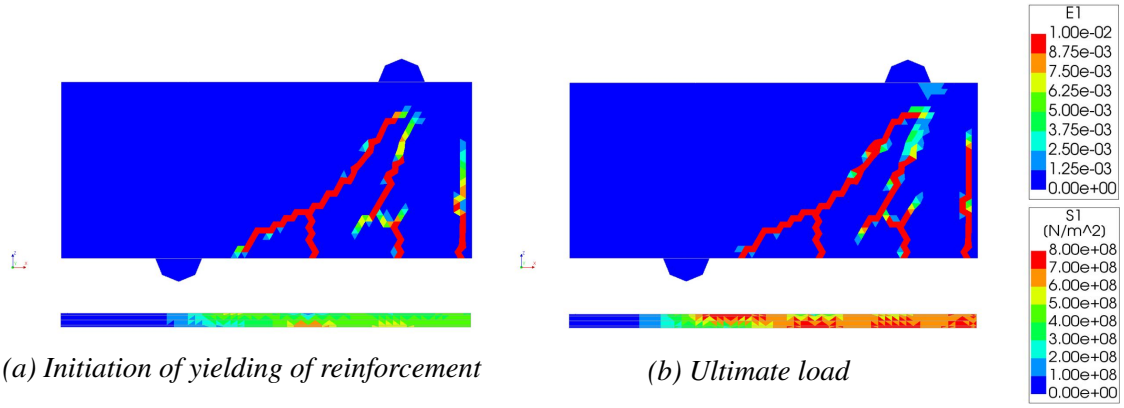

(a) Initiation of yielding of reinforcement *(b) Ultimate load*

Figure 3.20: Crack pattern for concrete class C50/60 with 55 µm (1.82%) corrosion.

The effect of increasing corrosion on the crack pattern is rather evident. An additional bending crack in the mid section occurs already at 25 μm (0.83%); at the level of 55 μm (1.82%), the first bending crack from the uncorroded state propagates towards a flexural shear crack. Furthermore, the inclined shear crack appears closer to the support with an increasing corrosion level and the crack path is more bent. The crack pattern development with increasing corrosion is different from the analysis of the original concrete strength. The most significant change is for the case with 55 μm (1.82%), with absence of the crack propagation along the reinforcement that occurs for the original concrete strength. For C50/60 this propagation is instead directed towards the lower edge in an inclined direction as a continuation of the shear crack. This results in a longer anchorage length available in comparison to the original concrete strength. For the corroded cases the stiffness is slightly higher than for the uncorroded after the first cracks occur, as shown in Figure 3.21. Moreover, the ultimate load capacity is almost unaffected by corrosion as presented in Table 3.12.

Table 3.12: Load levels for shear cracking, initiation of yielding in the reinforcement, and ultimate load for the FE model with concrete class C50/60

Corrosion level	Shear crack [kN]			Yielding [kN]	Ultimate load [kN]
	1^{st}	2^{nd}	3^{rd}		
No corrosion (0%)	127.2			178.6	251.2
25 μm corrosion (0.83%)	116.5	122.2	190.4	170.7	249.4
55 μm corrosion (1.82%)	97.1	108.3		177.1	250.1

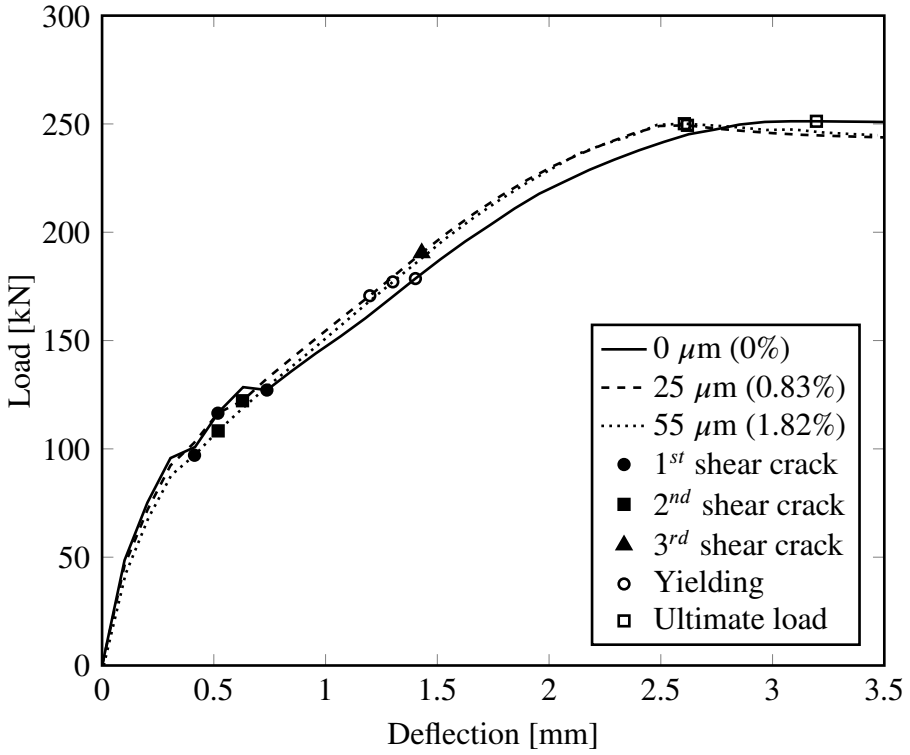

Figure 3.21: Load-deflection curves for different corrosion levels with markers for important load levels.

Concrete class C30/37

For the analyses with the lower concrete strength, C30/37, a different method for solving the equation iterations was required to reach convergence in the mechanical loading phase for the corroded cases. The method BFGS was chosen instead of Newton-Raphson; except from the iteration method itself all the other analysis settings listed in Figure 3.9 were kept. Crack patterns for the three analyses with corrosion levels are displayed in Figures 3.22, 3.23, and 3.24.

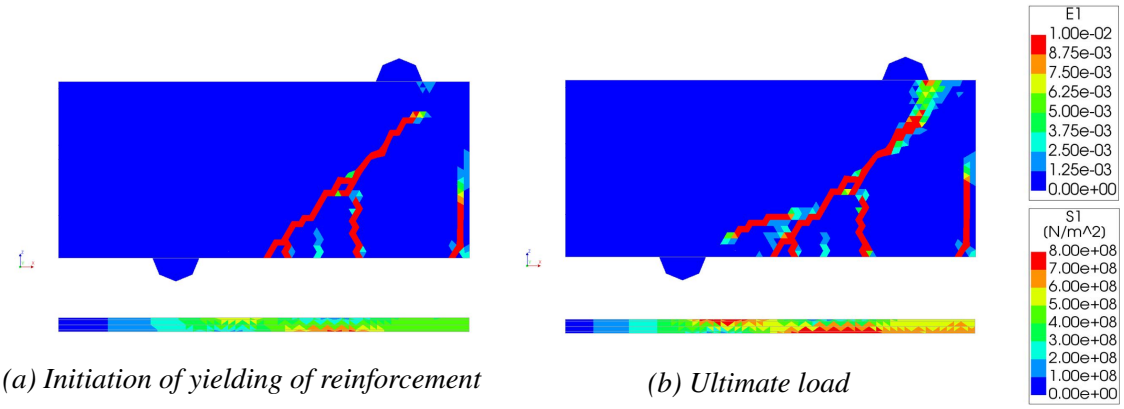

(a) Initiation of yielding of reinforcement *(b) Ultimate load*

Figure 3.22: Crack pattern for concrete class C30/37 without corrosion.

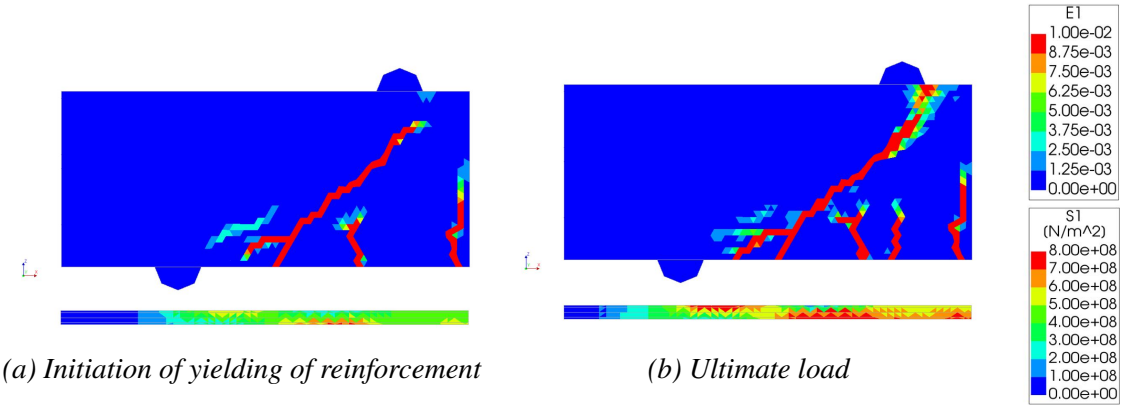

(a) Initiation of yielding of reinforcement *(b) Ultimate load*

Figure 3.23: Crack pattern for concrete class C30/37 with 25 µm (0.83%) corrosion.

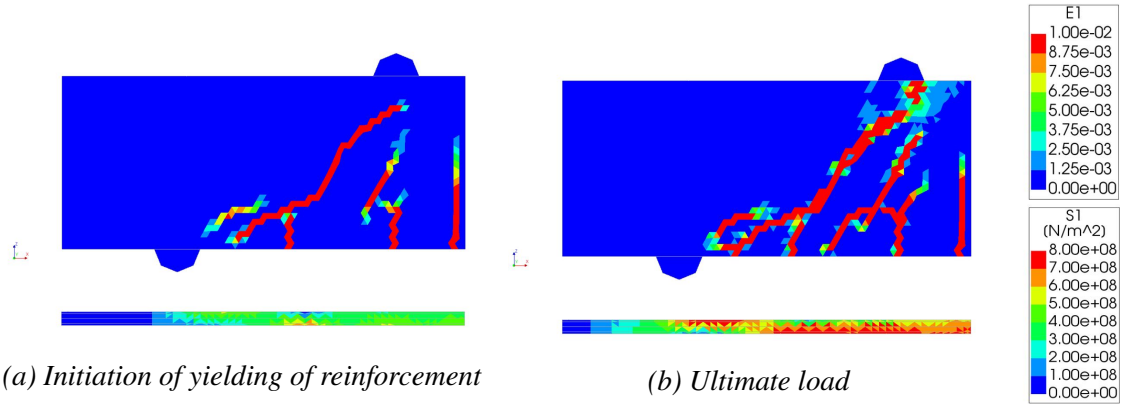

(a) Initiation of yielding of reinforcement *(b) Ultimate load*

Figure 3.24: Crack pattern for concrete class C30/37 with 55 µm (1.82%) corrosion.

A pervading trend for the crack pattern of the concrete class C30/37 is that with increased corrosion, the cracks are more numerous, in regard of both shear- and bending cracks. At a level of 25 μm (0.83%) corrosion, there is a distinct crack along the reinforcement towards the support with two additional shear cracks that emanates from the horizontal crack. However, in contrast to what could expect with regards to the trend of the other analyses compared, this behaviour is less distinguished for the level of 55 μm (1.82%) corrosion. Although, at the section of the loading point, there is an extra shear crack for this level of corrosion. The ultimate load is enhanced with increased corrosion as shown in Table 3.13. Furthermore, the stiffness is slightly higher for larger deflections as displayed in Figure 3.25. After the first shear cracks there are larger stiffness reductions in the cases with 0 and 25 μm (0.83%) compared to the most corroded. However, the highest corrosion level gives a higher stiffness after the shear cracks occur, and reaches in the end also a higher load capacity.

Table 3.13: Load levels for shear cracking, initiation of yielding in the reinforcement, and ultimate load for the FE model with concrete class C30/37

Corrosion level	Shear crack [kN]				Yielding [kN]	Ultimate load [kN]
	1^{st}	2^{nd}	3^{rd}	4^{th}		
No corrosion (0%)	99.0	191.3			163.2	196.2
25 μm corrosion (0.83%)	110.4	169.1			169.1	202.0
55 μm corrosion (1.82%)	97.4	103.3	111.8	128.0	155.6	211.7

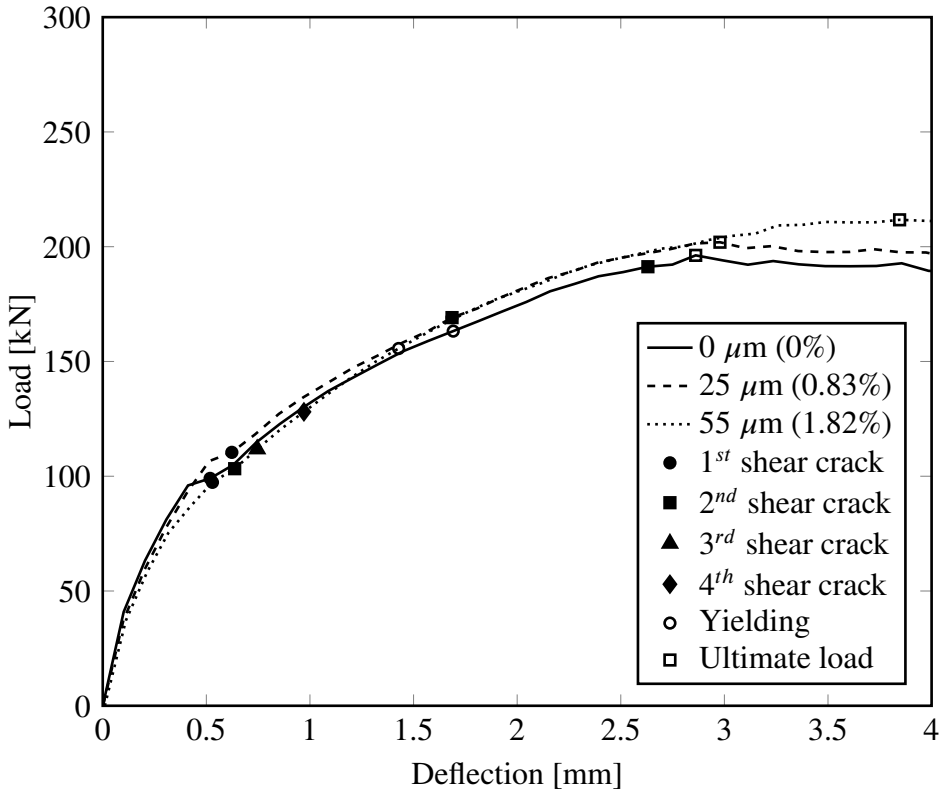

Figure 3.25: Load-deflection curves for different corrosion levels with markers for important load levels.

3.2.4 Variation of span length

The original shear span of the beam was 190 mm which results in a shear span ratio of 1.58. For the comparison, one longer span was modelled. In order to get a suitable shear span ratio for the longer beam model the shear span was chosen as 2.0, which resulted in a span length of 240 mm. For the analyses with corrosion, a different iteration method was required to reach convergence where BFGS was used instead of Newton-Raphson. For the different corrosion levels the crack patterns is displayed in Figure 3.26, 3.27, and 3.28.

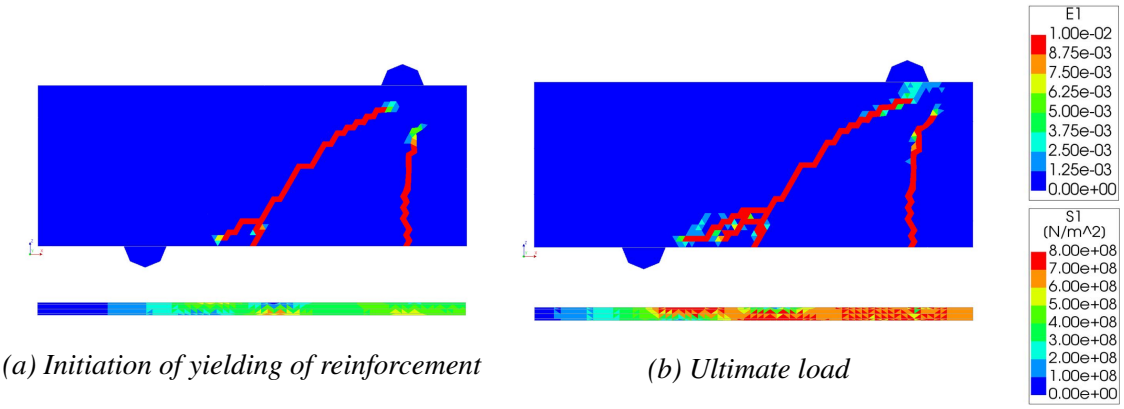

(a) Initiation of yielding of reinforcement *(b) Ultimate load*

Figure 3.26: Crack pattern for the case without corrosion.

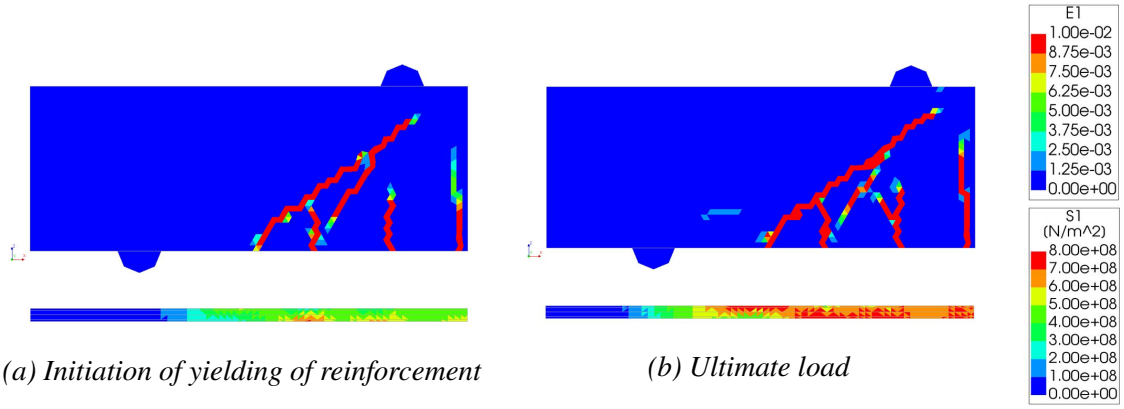

(a) Initiation of yielding of reinforcement *(b) Ultimate load*

Figure 3.27: Crack pattern for 25 µm (0.83%) corrosion.

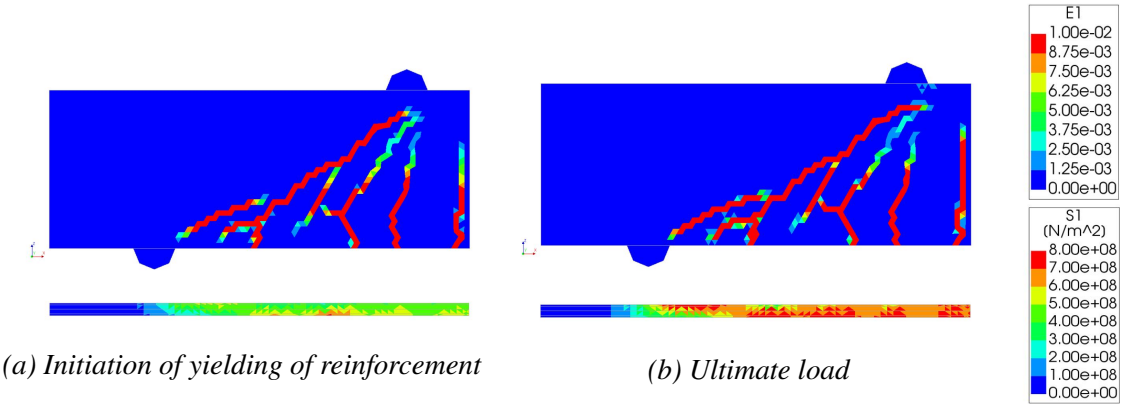

(a) Initiation of yielding of reinforcement *(b) Ultimate load*

Figure 3.28: Crack pattern for 55 µm (1.82%) corrosion.

Both span lengths show similar behaviour for the uncorroded cases. The bending crack is localised arguably at the same place and the shear crack have approximately the same shape but is extended due to the longer shear span. The exception is for the part between the lower edge and the longitudinal reinforcement, where additional cracks are present for this case and they reach considerably closer to the support than for the original beam. With increased corrosion there are several extra bending- and shear cracks. For the highest corrosion level, horizontal cracks develops at the level of the reinforcement but is more distinguished a bit further above in the cross section. Although, for the case with 55 μm (1.82%) corrosion, there are two larger shear cracks where the left one, the dominating, has an intersection point at roughly the same place as for the uncorroded case.

For 25 μm (0.83%) corrosion and the uncorroded case, there is a noticeable reduction of the stiffness when the first shear crack occurs and for the uncorroded case, a similar reduction also occurs earlier at the load level of the first bending crack, at approximately 95 kN. However, such a breaking point is not present for the case with 55 μm (1.82%) as displayed in Figure 3.29. Instead the curve is a bit bent following the stiffness reduction due to the shear cracks. Regarding the ultimate load, it is similar for the different corrosion levels as Table 3.14 shows.

Table 3.14: Load levels for shear cracking, initiation of yielding in the reinforcement, and ultimate load for the FE model with longer shear span

Corrosion level	Shear crack [kN]				Yielding [kN]	Ultimate load [kN]
	1^{st}	2^{nd}	3^{rd}	4^{th}		
No corrosion (0%)	122.4	120.7	159.2		139.0	208.1
25 μm corrosion (0.83%)	124.5	133.2			158.9	210.1
55 μm corrosion (1.82%)	109.4	116.7	128.5	137.8	158.8	210.4

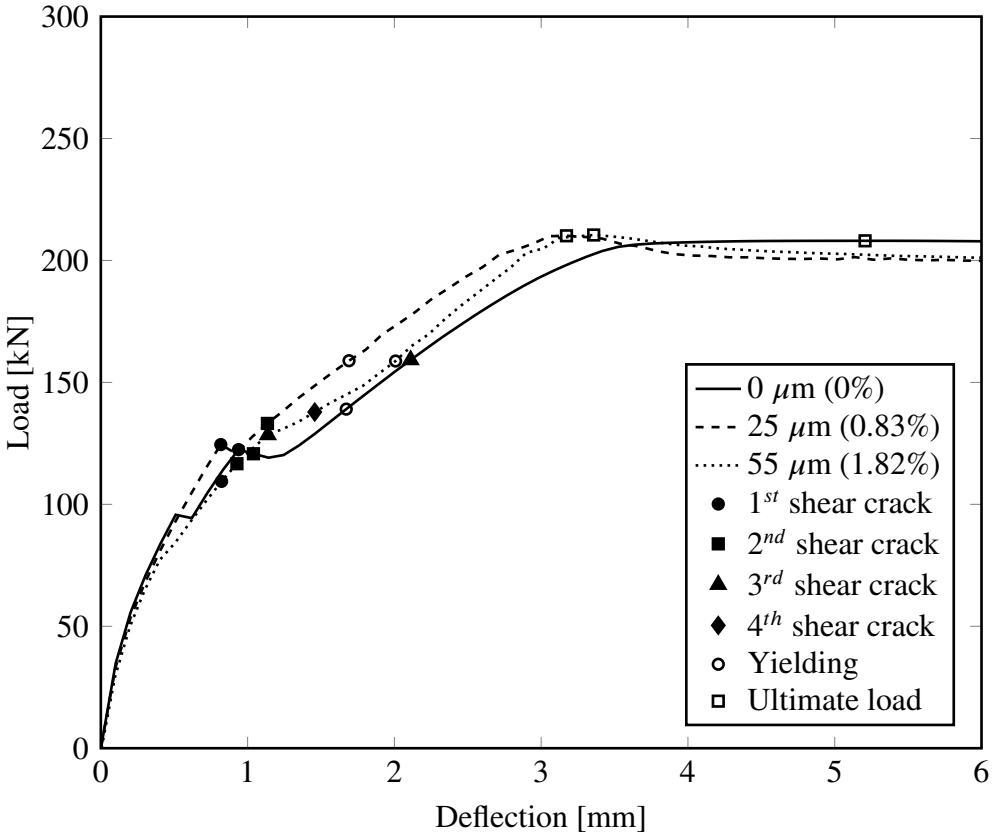

Figure 3.29: Load-deflection curves for different corrosion levels with markers for important load levels.

3.2.5 Influence of transverse reinforcement

The stirrups are designed according to the minimum requirements of Eurocode 2 (2004). Using the concrete class and a chosen bar diameter of 6 mm, it is possible to determine a maximum spacing between the stirrups; this distance is 90 mm, and the calculations are presented in Appendix A. The material properties for the stirrups are the same as for the longitudinal reinforcement, see Table 3.7, but the stirrup are modelled as embedded reinforcement elements in the FE model. This means that the reinforcement is modelled inside the concrete elements and adapts to the surrounding concrete mesh with perfect bond between the two materials. Figure 3.30 displays the cross-sections of the modelled beam with stirrups and Figures 3.31, 3.32, and 3.33 show the crack patterns for the three corrosion analyses.

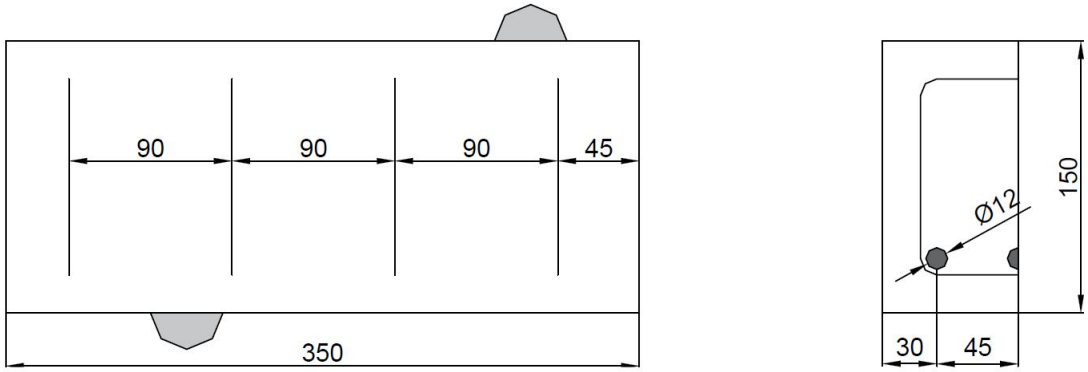

Figure 3.30: Dimensions of the beam model with stirrups.

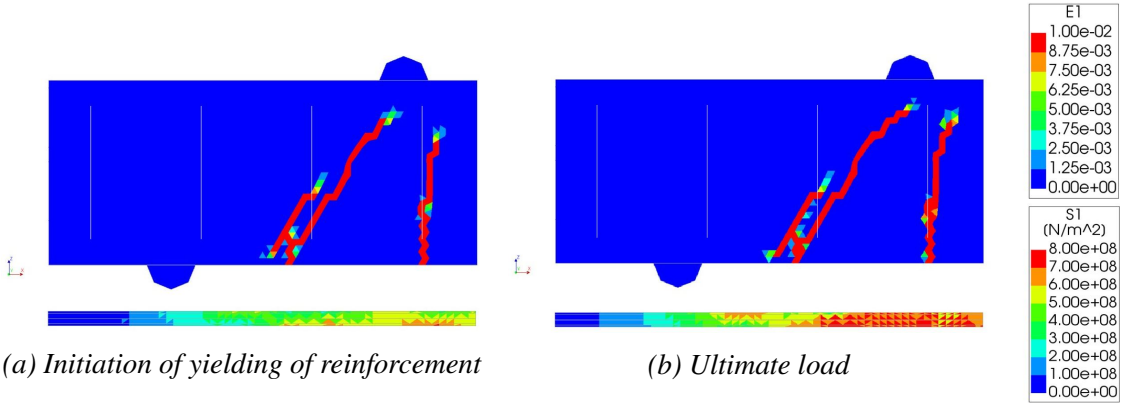

(a) Initiation of yielding of reinforcement *(b) Ultimate load*

Figure 3.31: Crack pattern for the case without corrosion.

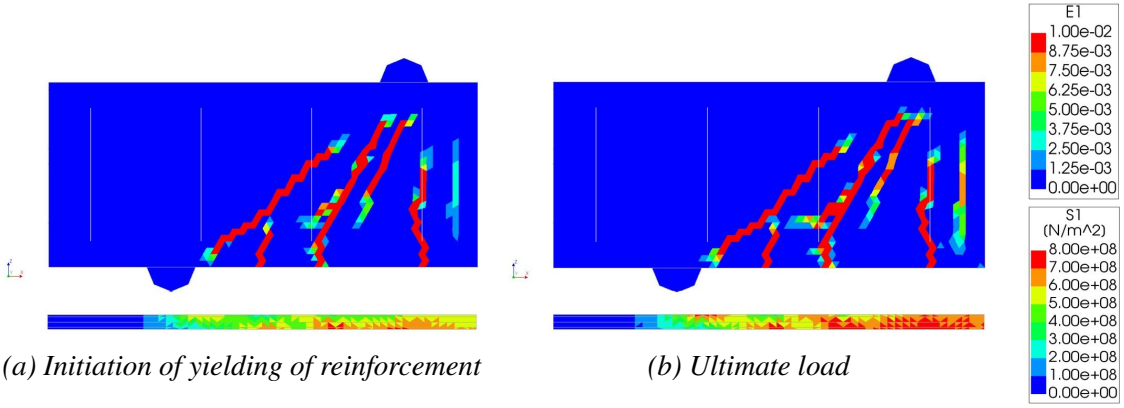

(a) Initiation of yielding of reinforcement *(b) Ultimate load*

Figure 3.32: Crack pattern for 25 µm (0.83%) corrosion.

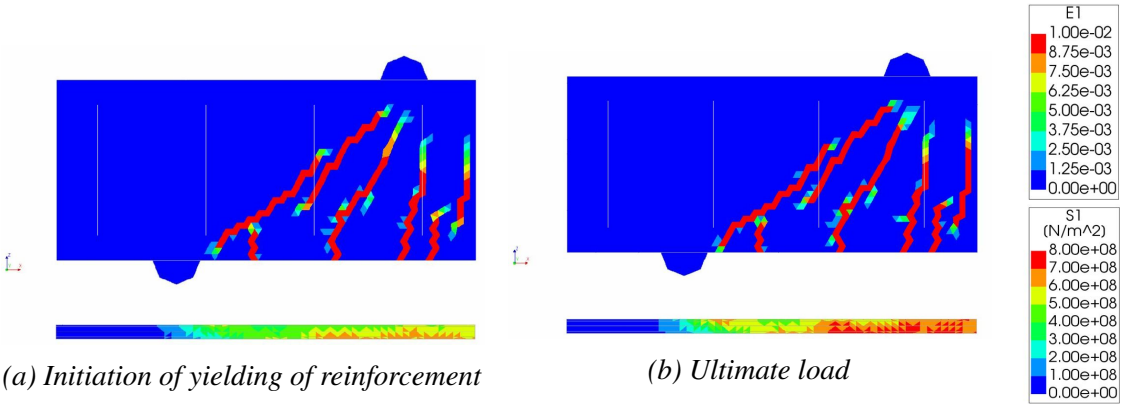

(a) Initiation of yielding of reinforcement *(b) Ultimate load*

Figure 3.33: Crack pattern for 55 µm (1.82%) corrosion.

There is a significant development of the crack pattern with increased corrosion for the analyses with stirrups. A second shear crack with less inclination appear close to the support for both cases with corrosion. For the one with 55 μm (1.82%) corrosion the second and third shear crack, the ones to the left, is initiated at the same time and at the level of the ultimate load they are arguable connected and could perhaps be considered as only one. At the same level of corrosion, two additional bending cracks in the mid section appears. Another behaviour, which follows the general ones, is the stiffness reduction in form of a breaking point due to cracking. For the uncorroded case a stiffness reduction occurs first for the first bending crack and then due to the first shear crack which is shown in Figure 3.34. Regarding the case with 25 μm (0.83%) corrosion, this reduction occurs first at the third shear crack. Furthermore, for 55 μm (1.82%) corrosion such a distinct change of stiffness is absent, even though a slight reduction occurs.

Table 3.15: Load levels for shear cracking, initiation of yielding in the reinforcement, and ultimate load for the FE model with stirrups

Corrosion level	Shear crack [kN]			Yielding [kN]	Ultimate load [kN]
	1^{st}	2^{nd}	3^{rd}		
No corrosion (0%)	146.3	156.0		210.1	260.3
25 μm corrosion (0.83%)	128.7	142.2	159.2	226.5	270.9
55 μm corrosion (1.82%)	137.1	160.3	160.3	228.5	266.8

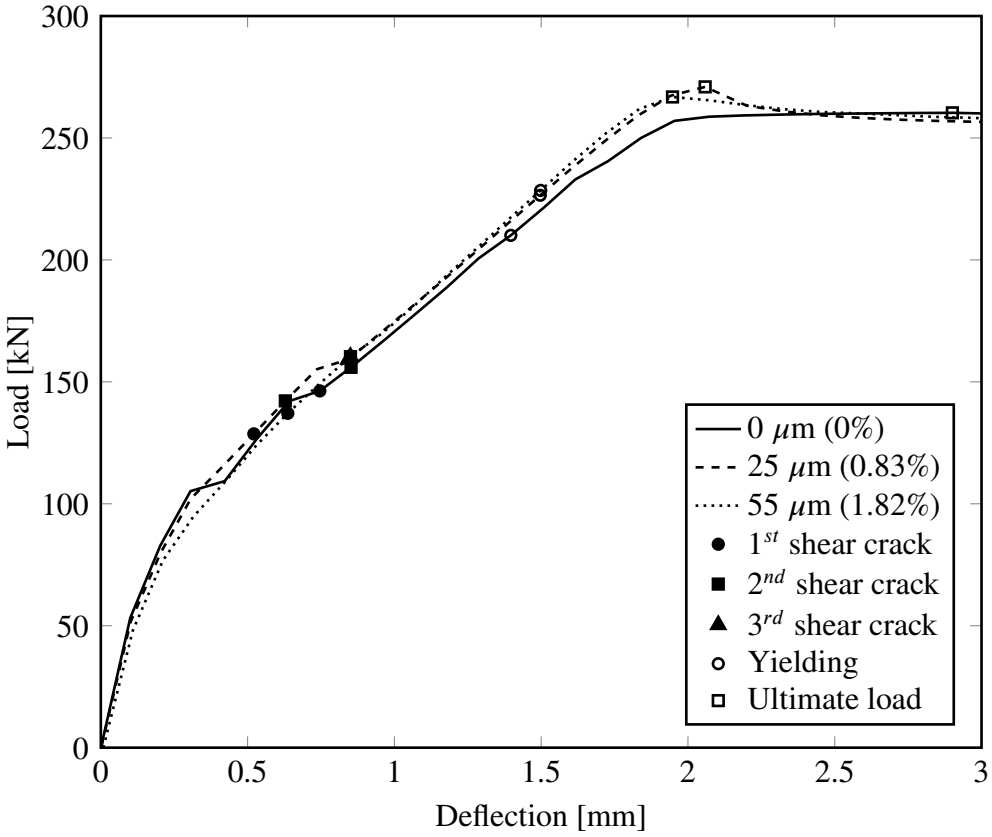

Figure 3.34: Load-deflection curves for different corrosion levels with markers for important load levels.

3.2.6 Summary of the shear crack angle development

The shear crack angles from the parametric study is summarised in Table 3.16. There is a pervading trend of a decreased angle with increased corrosion which is most pronounced for the analysis that includes stirrups. The angle is measured from a point where the dominating shear crack intersect with the reinforcement, to a point at the top of the shear crack. All figures of crack pattern including the measurement of the angles is collected in Appendix B.

Table 3.16: Shear crack angle development

Corrosion level	Analysis				
	Original	C50/60	C30/37	Longer span	Stirrups
No corrosion (0%)	46°	45°	44°	39°	51°
25 μm corrosion (0.83%)	42°	42°	42°	37°	47°
55 μm corrosion (1.82%)	42°	41°	42°	34°	38°

3.3 Induced stresses in stirrups due to corrosion of main bar

The second focal point of this Master's thesis is the phenomenon where the corroding, thus expanding, longitudinal reinforcement induces stresses in the adjacent stirrups. The induced tensile stresses reduce the available shear capacity and because of this, these stresses are of great interest to be quantified for different levels of corrosion. The stirrup arrangement is the same as presented in Section 3.2.5, but these analyses, are run for a larger variety of corrosion levels. It is more extensive, meaning that a considerable higher levels of corrosion are included in these analyses. For this reinforcement arrangement, the highest corrosion level that affects the friction is 500 μm (15.97%), the reason is the bond/corrosion model described in Section 2.4.1, which applies the same friction coefficient for all values above. However, at higher corrosion levels the reduction of the cross-section for the reinforcement continues if this phenomena was included in the model. The FE model was able to continue to a corrosion level slightly above 200 μm (6.56%), which therefore was decided as the maximum level for the analysis. Thereby, the corrosion levels listed in Table 3.17 are compared in these analyses. However, the highest corrosion level, 6.56%, is considered to a high corrosion level compared to corroded RC structures in reality.

Table 3.17: Corrosion levels in the analysis

Corrosion penetration [μm]	Weight loss [%]
50	1.66
100	3.31
150	4.94
200	6.56

For these analyses, neither self-weight nor mechanical loading was included since the focal point was to determine the stresses induced by corrosion only. The input parameters for this analyses are listed in Table 3.18. The material and dimensional parameters are the same as for the case with stirrups in the parametric study, see Section 3.2.5.

Table 3.18: Input parameters for the corrosion induced stresses analysis

Corrosion	
Time dependent increment	1 μm/s
Iterative method	Newton Raphson
Maximum number of iterations	100
Convergence norm (tolerance)	Force (10^{-2})
	Displacement (10^{-2})
Abort criterion	10^{40}
If no convergence	Continue

The area where the corrosion-induced stresses in the stirrups were monitored was limited to the part in connection to the longitudinal reinforcement i.e. the horizontal part in the bottom, the lower left corner, and the vertical part closest to the corroded reinforcement, see Figure 3.35. The upper parts did

not interact with the corroded reinforcement and was therefore not included. The difference in stresses between the four stirrups was very small and it was therefore chosen to only present one of them, namely the stirrup closest to the center of the beam. In the DIANA software there is an inbuilt function to determine the stresses in the embedded elements in the different directions, x, y, and z, which has been used. Stresses along the bar, σ_Y and σ_Z, can be implemented directly for the horizontal respective the vertical part of the stirrup. For the inclined part around the main bar, the two stresses are combined to give the stress along the stirrup.

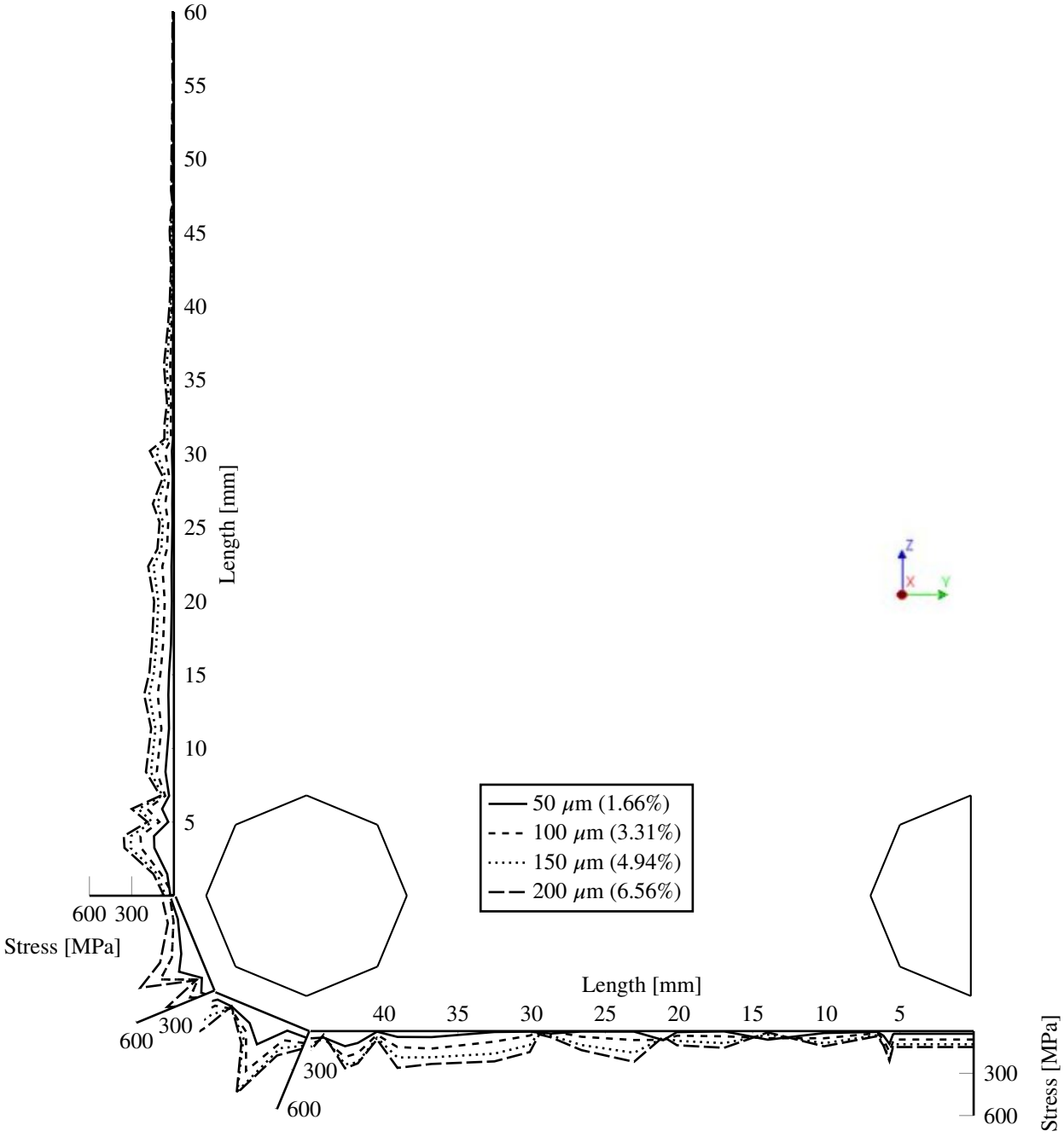

Figure 3.35: Corrosion-induced stresses along the stirrup.

The stresses induced in the stirrups due to corrosion of the longitudinal reinforcement are high, even close to yielding, as Figure 3.35. For the highest corrosion level, the stresses reach close to yielding, 700 MPa. This is however very locally, as shown in Figure 3.36a, and could be explained by the fact that the stirrup elements are modelled with embedded elements in the FE model. The element lengths along the stirrups are depending on the surrounding concrete and are thereby unevenly distributed. There is full interaction between the concrete and stirrups and the reinforcement stresses are calculated on the stress-strain relation. If a bond model was to be implemented the stirrup stresses would probably be more distributed and the peaks would be less distinguished. The stirrup stresses are shown in Figure 3.36. When the local maximums are compared with the crack pattern in Figure 3.37, it is noticed that the position of these sections coincide with the most pronounced corrosion induced cracks around the longitudinal reinforcement.

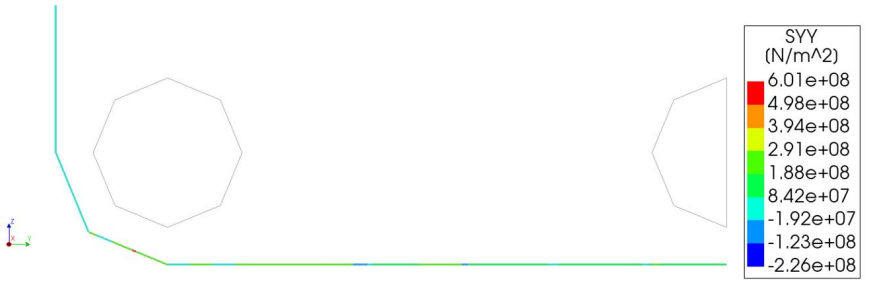

(a) Corrosion induced stresses σ_{yy}

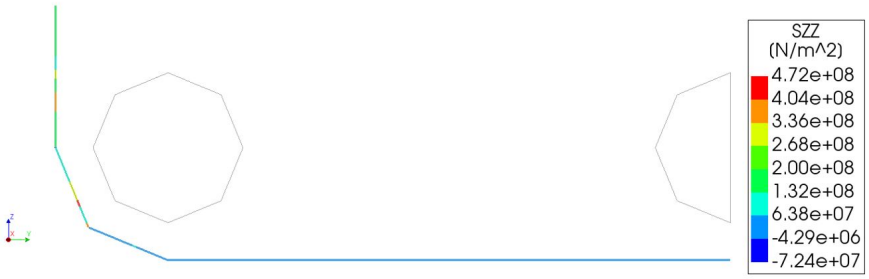

(b) Corrosion induced stresses σ_{zz}

Figure 3.36: Corrosion induced stresses from FE analysis

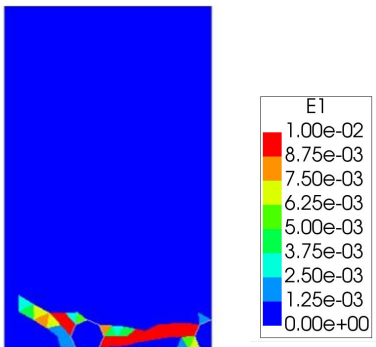

Figure 3.37: Crack pattern for induced stresses at 200 µm (6.56%) corrosion.

4 Discussion

During the initial process of verification of the FE model, which is described in Section 3.2.1, the most important factors for the comparison with the experimental test were the ultimate load capacity and the crack pattern. Several parameters were changed in order to get a realistic behaviour compared to the experiments by RISE and CBI. In terms of the load step size it is important to use a sufficient small one to obtain a good balance between accurate results and computational time. However, during the process of finding the optimal one, a factor of uncertainty appeared unexpected. A step size of 0.1 mm resulted in a desired crack pattern and ultimate load capacity, but for half the step size and otherwise the same input parameters, a different crack pattern was obtained. The same behaviour took place for twice the step size, i.e. 0.2 mm. The FE model was checked carefully, since this behaviour was unexpected, without any success of describing the reason. Although, it is possible that the crack pattern may vary for different load increments. A crack could be localized at different places during iteration towards equilibrium for different load increments, meaning that the crack propagation could be dependent on the size of the load increments. Furthermore, the bond model by Lundgren (2005a) were, according to Zandi Hanjari (2010), calibrated for pull-out tests with anchorage failure, meaning that for small bond slips as in this study the bond model might be slightly incorrect.

The ultimate load capacity of the models was for some parameters slightly higher with increased corrosion level. The reason that corrosion is a bit favourable in this regard could be due to the friction factor in the bond model described in Section 2.4.1, which for these corrosion levels means a higher bond capacity in terms of friction as showed in Figure 4.1.

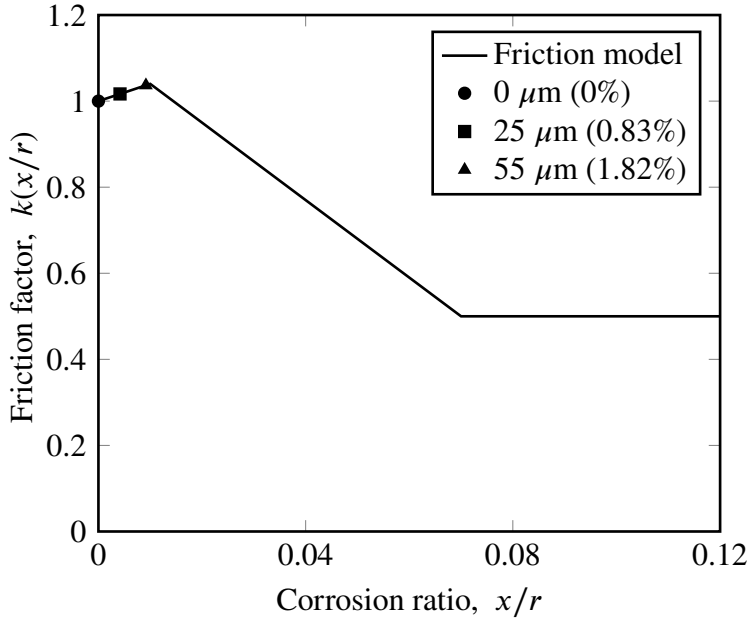

Figure 4.1: Friction model according to Lundgren (2005b) with markers for the compared corrosion levels.

Furthermore, in this thesis the reduction of the reinforcement steel area due to corrosion is not included. For the bond model applied, this have to be done manually in the FE analysis and would probably result in a slightly lower ultimate loads for the corroded cases. But since the scope was to determine the shear crack angles, the load levels were not considered as important.

In the study made by Zandi (2014b) concerning the corrosion induced stresses in the stirrups, the resulting maximum induced stress was 80 MPa while this thesis presents results of stresses up to 600 MPa. Except from obvious differences in the studies regarding the beam dimensions and input parameters, an important differing factor is how the stirrups were modelled. Zandi's model included a bond model on the stirrups and also modelled them as solid continuum 3D elements with concrete elements in between the longitudinal reinforcement and the stirrups. With an applied bond model, the stresses along the stirrups would be more evenly distributed.

A decreasing shear crack angle with increased corrosion, as the result from this thesis indicates, means that a larger stress component is carried in the longitudinal reinforcement instead of the transverse. This will also mean that there will be larger stresses in the concrete compression struts. As a consequence of this the longitudinal reinforcement have to transfer larger forces while the capacity of the reinforcement is decreased, in terms of reduced cross-section due to rust.

5 Conclusions and further research

5.1 Conclusions

Based on the results from the parametric study of the shear crack response on RC structures subjected to corrosion, mainly three observations can be made; change of the shear crack angle, development of the crack pattern, and increased ultimate load capacity. A comprehensive comparison of how the shear crack angle is changing with regard to the different parameters is summarized in Appendix B. The angle is measured for the dominating shear crack between the intersection with the reinforcement to a point located on the top of the crack. The study showed a consistent result of a smaller angle to the longitudinal reinforcement with increased corrosion level for all compared parameters. The results also indicate that the most influential parameter is the presence of stirrups while different concrete strengths seem to affect the shear crack angle the least. A smaller shear crack angle means that a larger component of the stresses is carried by the compression strut and the longitudinal reinforcement in the strut-and-tie model, and the vertical stresses in the stirrup will therefore be smaller. Since this analysis only comprises corrosion of the longitudinal reinforcement, no significant reduction of the shear capacity was observed.

Regarding the amount of cracks, there is a pervading trend that increased corrosion gives a more extensive crack pattern, in terms of more shear- and bending cracks. Unlike the shear crack angle, the different parameters had less influence on the number of cracks. The ultimate load capacity of the models was for some parameters higher with increased corrosion level. A trend in the analyses is that the first visible shear crack occurred at a lower load for the models with the highest corrosion level compared to the uncorroded ones. This difference is particularly significant for the reference model, the one with concrete class C30/37, and the one with longer shear span. In some of the cases, the first shear crack is not the dominating one and it is therefore difficult to draw any major conclusions from this, except that corrosion accelerates the shear cracking process.

A similar investigation to this Master's thesis second focal point concerning corrosion induced stresses by Zandi (2014b) studied pull-out specimens with a corrosion weight loss up to 20%. These results showed that induced stirrup stresses reached around 80 MPa due to corrosion of the longitudinal reinforcement. However, the result of this work shows that corrosion on the longitudinal reinforcement significantly influences the stresses in the stirrups. In sections where a crack due to the expansion of rust appears, the stirrup stresses could reach close to the yield strength. In contrast to what the paper by Zandi (2014b) proposes, these results indicates that the stresses induced from corrosion may affect the shear capacity of the RC member significantly. However, there are some differences between the analyses; the beam and reinforcement dimension and arrangement, but also that the reinforcement and stirrups were modelled as solid elements in the FE software. This allows the FE model to include a bond model for the stirrups, meaning that the influence of corrosion on the stirrups is regarded as well.

The results from this study indicates that corrosion on the longitudinal reinforcement decreases the shear crack angle and also results in a more extensive crack pattern. Additional cracks could be regarded as favourable from a structural stand point, if the total crack widths are more evenly distributed over the beam. Furthermore, the results from this thesis indicate that the shear capacity of the stirrups

could be significantly affected by corrosion of the longitudinal reinforcement. A quantification of these phenomenons' total influence could be implemented in a simple-to-use modelling tool. Such tool would improve the assessment of the remaining capacity of corroded RC structures and this could lead to great public savings. Results from this Master's thesis are meant to be included in a 1D-model developed at Chalmers referred to as ARC.

5.2 Further research

To get more understanding of the influence of corrosion on the shear crack angle it is of interest to include corrosion of the stirrups as well. It is also of interest to include more parameters to the study, such as different bar diameters and different reinforcement arrangements. The dimensions of the studied beam is small for efficiency when conducting the parametric study, but in order to give a representative recommendation regarding the shear crack angle, larger beams should also be investigated. But since the experiment that the results were verified against also is from a small beam, further experiments with other dimensions should be carried out. The results indicate that presence of stirrups affected the shear crack angle a lot, therefore it would be interesting to also study different stirrup arrangements. It would also be of interest to continue the parametric study with higher corrosion levels, resulting in spalling of concrete. To get a clearer view regarding how the different parameters interact with each other, further analyses could be done with different combinations of the parameters. A study using e.g. a factorial design could be carried out to investigate these interactions. Finally, the results from the study indicates that corrosion means a smaller shear crack angle but in order to use this information for future assessments guidelines, the effect needs to be quantified with more analyses and also physical experiments. The analyses in Section 3.3 also needs to be re-run with a bond model included for the stirrups as well.

Bibliography

Bell, B. (2004). “Sustainable bridges. D1.3 European Railway Bridge Problems”. In: (cit. on pp. 1, 5).

Cairns, J., G. A. Plizzari, Y. Du, D. W. Law, and C. Franzoni (2005). “Mechanical properties of corrosion-damaged reinforcement”. In: *ACI Materials Journal* 102.4 (cit. on p. 7).

Chen, J. (2002). “Study on durability of concrete members due to reinforcement steel corrosion”. In: *Cem. Concr. Composites* 18 (cit. on p. 7).

DIANA (2017). *DIANA Finite Element Analysis, User’s Manual, Release 10.1* (cit. on p. 19).

Du, H. and N. Chen (2012). *Detailed Study of the Cracking Process at Shear Failure through FE Analysis of Beam Experiments*. Tech. rep. Department of Civil and Environmental Engineering (cit. on pp. 10, 11, 18, 19, 22).

Du, Y. G., L. A. Clark, and A. H. C. Chan (2005). “Effect of corrosion on ductility of reinforcing bars”. In: *Magazine of Concrete Research* 57.7 (cit. on p. 7).

Al-Emrani, M., B. Engström, M. Johansson, and P. Johansson (2013). *Bärande konstruktioner, Del 1* (cit. on pp. 3, 4).

Engström, B. (2015). *Design and analysis of deep beams, plates and other discontinuity regions* (cit. on pp. 4, 5).

Eurocode 2 (2004). *Eurocode 2: Design of concrete structures - Part 1-1: General rules and rules for buildings, EN 1992-1-1:2004: E* (cit. on pp. 4, 17, 40).

Fernandez Perez, I., M. Tahershamsi, A. Marí, J. Bairán, K. Lundgren, K. Zandi, and M. Plos (2014). “1D and 3D analysis of anchorage in naturally corroded specimens”. In: (cit. on p. 6).

fib (2000). *Bond of Reinforcement in Concrete, State-of-art report* (cit. on p. 7).

fib Model Code (1990). *fib Model Code for Concrete Structures 1990* (cit. on pp. 6, 22).

– (2010). *fib Model Code for Concrete Structures 2010, Chapter 5.1.5.2 Fracture energy* (cit. on pp. 22, 30).

Flansbjer, M., J. Lindqvist, and J. Silfwerbrand (2011). *Quantitative fracture characteristics in shear load* (cit. on p. 10).

Higgins, C. and W. C. Farrow (2006). “Tests of reinforced concrete beams with corrosion-damaged stirrups”. In: *ACI Structural journal* 103.1 (cit. on p. 6).

Hordijk, D. A. (1991). *Local Approach to Fatigue of Concrete*. Tech. rep. (cit. on p. 19).

Juarez, C., B. Guevara, G. Fajardo, and P. Castro-Borges (2011). “Ultimate and nominal shear strength in reinforced concrete beams deteriorated by corrosion”. In: (cit. on p. 6).

Khan, I., R. Francois, and A. Castle (2013). “Experimental and analytical study of corroded shear-critical reinforced concrete beams”. In: *Materials and Structures* (cit. on p. 6).

Lundgren, K. (2002). “Modelling the effect of corrosion on bond in reinforced concrete”. In: *Magazine of Concrete Research* 54.3 (cit. on p. 9).

– (2005a). “Bond between ribbed bars and concrete. Part 1: Modified model”. In: *Magazine of Concrete Research* (cit. on pp. 2, 7–9, 11, 12, 49).

– (2005b). “Bond between ribbed bars and concrete. Part 2: The effect of corrosion”. In: *Magazine of Concrete Research* 7 (cit. on pp. 5, 7–9, 12, 24, 49).

– (2007). “Effect of corrosion on the bond between steel and concrete: an overview”. In: *Magazine of Concrete Research* 6 (cit. on p. 7).

Lundgren, K. and K. Gylltoft (2000). “A model for the bond between concrete and reinforcement”. In: *Magazine of Concrete Research* 52.1 (cit. on pp. 7, 8, 11).

Lundgren, K., P. Kettil, K. Zandi Hanjari, H. Schlune, and A. Soto San Roman (2012). “Analytical model for the bond-slip behaviour of corroded ribbed reinforcement”. In: *Structure and Infrastructure Engineering* 8 (cit. on p. 6).

Lundgren, K., U. Nilsson, R. Ronnebrant, and A. Maglica (2014). “Bärighetsutredning av betongbroar med rostande armering”. In: 7 (cit. on pp. 1, 5, 6).

Lundgren, K., M. Tahershamsi, K. Zandi, and M. Plos (2014). “Tests on anchorage of naturally corroded reinforcement in concrete”. In: *Materials and Structures* (cit. on pp. 6, 7, 9, 10, 12).

Nilsson, U. and K. Lundgren (2014a). “Blommenbergsviadukten, 2-2033-1. Kompletterande bärighetsutredning med avseende på kontroll av kapacitet i gjutfogar baserat på beräkningsmodell utvecklad av Chalmers tekniska högskola”. In: (cit. on pp. 1, 5, 6).

– (2014b). “Gröndalsviadukten, 2-2034-1. Kompletterande bärighetsutredning med avseende på kontroll av kapacitet i gjutfogar baserat på beräkningsmodell utvecklad av Chalmers tekniska högskola”. In: (cit. on pp. 1, 5, 6).

Palsson, R. and M. S. Mirza (2002). “Mechanical response of corroded steel reinforcement of abandoned concrete bridge”. In: *ACI Materials Journal* 99.2 (cit. on p. 7).

Petre-Lazar, I. (2000). *Evaluation du comportement en service des ouvrages en beton arme soumis a la corrosion des aciers(Aging assessment of concrete structures submitted to steel corrosion)* (cit. on p. 9).

Regan, P. and I. Kennedy-Reid (2009). *Assessment of concrete structures affected by delamination: 1 - Effect of bond loss* (cit. on p. 7).

Rodriguez, J., L. Ortega, and J. Casal (1997). “Load carrying capacity of concrete structures with corroded reinforcement”. In: *Const. Build. Mater.* 11 (cit. on p. 7).

Schlaich, J., K. Schäfer, and M. Jennewein (1987). “Toward a concistent design of structural concrete”. In: *PCI Journal* 32.2 (cit. on p. 4).

Selby, R. G. and F. J. Vecchio (1993). “Three-dimensional Constitutive Relations for Reinforced Concrete”. In: (cit. on p. 19).

Shu, J., D. Fall, M. Plos, K. Zandi, and K. Lundgren (2015). “Development of modelling strategies for two-way RC slabs”. In: *Engineering Structures* 101 (cit. on p. 18).

Taherhamsi, M., I. Fernandez, K. Zandi, and K. Lundgren (2016). “Four Levels to Assess Anchorage Capacity of Corroded Reinforcement in Concrete”. In: (cit. on pp. 9, 12–14).

Tahershamsi, M., K. Zandi, K. Lundgren, and M. Plos (2014). “Anchorage of naturally corroded bars in reinforced concrete structures”. In: *Magazine of Concrete Research* 14.66 (cit. on pp. 9, 12–14, 16).

Thorenfeldt, E., A. Tomaszewicz, and J. J. Jensen (1987). “Mechanical properties of high-strength concrete and applications in design”. In: *Conference on Utilization of High-Strength Concrete, Stavanger, Norway* (cit. on p. 19).

TNO (2017). *FE software DIANA 10.1* (cit. on pp. v, 12).

Wang, X.-H., X.-H. Gao, B. Li, and B.-R. Deng (2010). “Effect of bond and corrosion within partial length on shear behaviour and load capacity of RC beam”. In: *Construction and Building Materials* (cit. on p. 7).

Xu, S. and D. Niu (2004). “The shear behaviour of corroded simply supported reinforced concrete beam”. In: *J. Build. Struct.* 25 (cit. on p. 6).

Zandi Hanjari, K. (2010). *Structural Behaviour of Detoriated Concrete Structures*. Tech. rep. (cit. on pp. 1, 5, 49).

Zandi, K. (2014a). *1D-ARC PhD project description* (cit. on pp. 5, 6).

– (2014b). "Corrosion-induced cover spalling and anchorage capacity, Structure and Infrastructure Engineering: Maintenance, Management, Life-Cycle Design and Performance". In: (cit. on pp. 1, 6, 50, 51).

Zhang, R. (2008). "Analysis of Both Initiation and Propagation Phases of Corrosion in Reinforced Concrete Structures and Their Influence on Service Life". In: (cit. on p. 5).

Zhao, Y.-X., J. Chen, and W.-L. Jin (2009). "Design of shear strengths of corroded reinforced concrete beams". In: *Int. J. Modelling, Identification and Control* 7.2 (cit. on p. 6).

Zhao, Y.-X. (2002). *Effect of corrosion on bond behaviour and bending strength of reinforced concrete beams*. Tech. rep. Zhejiang University, Hangzhou, China (cit. on p. 7).

A Hand calculations

Design of stirrups

Eqiuations from the book "Bärande konstruktioner" by Al-Emrani, M. et al., (2013), based on Eurocode 2

Minimum transverse reinforcement (National parameter, recomended value). Originally based on steel yield strength of 500 MPa

$\rho_{w.min} := 0.00134$ Table B6.1

Bar diameter

$\phi := 6mm$

Cross-sectional bar area

$A_{sw} := \frac{\phi^2 \cdot \pi}{4} = 28.274334mm^2$

Beam width

$b_w := 150mm$

$d := 120mm$

Maximum stirrup spacing (National parameter, recomended value)

$s_{l.max} := 0.75 \cdot d = 90 \cdot mm$ (B6-26)

Stirrup spacing

$$s_{stirrups} := \min\left(\frac{A_{sw}}{\rho_{w.min} \cdot b_w}, s_{l.max}\right) = 90 \cdot mm$$

Fracture energy

Concrete compressive strengths (charasteristic values)

$f_{ck.71} := 71.83\,MPa$

$f_{ck.50} := 50MPa$

$f_{ck.30} := 30MPa$

$\Delta_f := 8MPa$

Concrete compressive strengths (mean values)

$f_{cm.71} := f_{ck.71} + \Delta_f = 79.83\ MPa$

$f_{cm.50} := f_{ck.50} + \Delta_f = 58\,MPa$

$f_{cm.30} := f_{ck.30} + \Delta_f = 38\,MPa$

Fracture energy accordeing to Model code 2010. Chapter 5.1.5.2

Original concrete strength

$$G_{F.71.2010} := 73\frac{N}{m}\cdot\left(\frac{f_{cm.71}}{MPa}\right)^{.18} = 160.6\cdot\frac{N}{m}$$ (5.1-9)

C50/60

$$G_{F.50.2010} := 73\frac{N}{m}\cdot\left(\frac{f_{cm.50}}{MPa}\right)^{.18} = 151.6\cdot\frac{N}{m}$$

C30/37

$$G_{F.30.2010} := 73\frac{N}{m}\cdot\left(\frac{f_{cm.30}}{MPa}\right)^{.18} = 140.5\cdot\frac{N}{m}$$

Fracture energy according to Model code 1990. DIANA FE Manual - Chapter 20.2.9.1
CEB-FIP Model Code 1990

$f_{cm0} := 10MPa$

Fine aggregate

$d_{max} := 8mm$ Table 20.1

$G_{F0} := 25\frac{N}{m}$

Original concrete strength

$$G_{F.71.1990} := G_{F0}\cdot\left(\frac{f_{cm.71}}{f_{cm0}}\right)^{.7} = 107.02\cdot\frac{N}{m}$$ (20.136)

C50/60

$$G_{F.50.1990} := G_{F0}\cdot\left(\frac{f_{cm.50}}{f_{cm0}}\right)^{.7} = 85.6\cdot\frac{N}{m}$$

C30/37

$$G_{F.30.1990} := G_{F0}\cdot\left(\frac{f_{cm.30}}{f_{cm0}}\right)^{.7} = 63.6\cdot\frac{N}{m}$$

Hardening curve for higher steel strength

Equations according to Annex C, Eurocode 1992-1-1

Yield and ultimate strength

$f_{y.550} := 550MPa$ $f_{u.550} := 630MPa$

Ratio between yeild and ultimate strength

$$k := \frac{f_{u.550}}{f_{y.550}} = 1.145$$

Control for steel class A

$k > 1.05 = 1$ Table C.1

Same ralation k between yield and ultimate strength for different yield strengths

$f_{y.600} := 600MPa$ $f_{u.600} := k \cdot f_{y.600} = 687.3 \cdot MPa$

$f_{y.650} := 650MPa$ $f_{u.650} := k \cdot f_{y.650} = 744.5 \cdot MPa$

$f_{y.675} := 675MPa$ $f_{u.675} := k \cdot f_{y.675} = 773.2 \cdot MPa$

$f_{y.690} := 690MPa$ $f_{u.690} := k \cdot f_{y.690} = 790.4 \cdot MPa$

$f_{y.700} := 700MPa$ $f_{u.700} := k \cdot f_{y.700} = 801.8 \cdot MPa$

Young's modulus of reinforcement steel

$E_s := 220GPa$

Yield- and ultimate strains to calculate the strains for the hardening curve of two steel strengths

$$\varepsilon_{y.550} := \frac{f_{y.550}}{E_s} = 2.5 \times 10^{-3}$$

$\varepsilon_{y.550.1} := \varepsilon_{y.550} + 0.07 = 0.0725$

$\varepsilon_{u.550} := \varepsilon_{y.550} + 0.125 = 0.1275$

$$\varepsilon_{y.700} := \frac{f_{y.700}}{E_s} = 3.182 \times 10^{-3}$$

$\varepsilon_{y.700.1} := \varepsilon_{y.700} + 0.07 = 0.0732$

$\varepsilon_{u.700} := \varepsilon_{y.700} + 0.125 = 0.1282$

B Shear crack angle

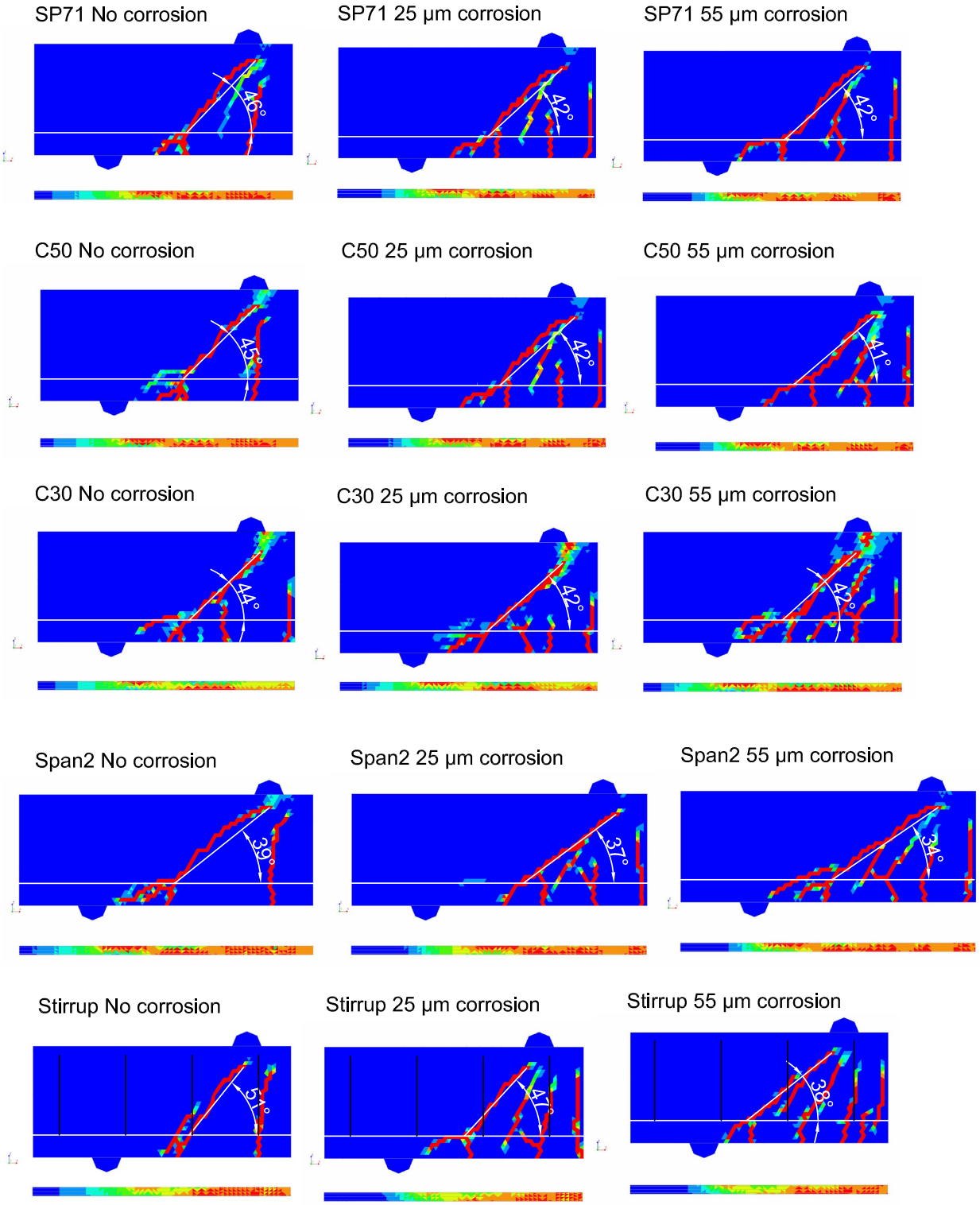

C Dat files from DIANA

```
                                    SP orginal
: Diana Datafile written by Diana 10.1
'DIRECTIONS'
   1   1.00000E+00   0.00000E+00   0.00000E+00
   2   0.00000E+00   1.00000E+00   0.00000E+00
   3   0.00000E+00   0.00000E+00   1.00000E+00
'MODEL'
DIMENS "3D"
GRAVDI 3
GRAVAC  -9.81000E+00
'COORDINATES'

'MATERI'
   1 NAME   "Concrete"
     MCNAME CONCR
     MATMDL TSCR
     YOUNG    3.95000E+10
     POISON   2.00000E-01
     DENSIT   2.40000E+03
     TOTCRK ROTATE
     CBSPEC ROTS
     TENCRV HORDYK
     POIRED NONE
     TENSTR   4.90000E+06
     GF1      2.0870E+02
     COMCRV THOREN
     REDCRV NONE
     CNFCRV VECCHI
     COMSTR   7.18300E+07
     LTHORE   3.00000E-01
     ASPECT
   2 NAME   "Reinforcement steel"
     MCNAME MCSTEL
     MATMDL TRESCA
     YOUNG    2.22000E+11
     POISON   3.00000E-01
     DENSIT   7.80000E+03
     YIELD  VMISES
     TRESSH KAPSIG
     HARDEN STRAIN
     KAPSIG   0.00000E+00   7.00000E+08   7.00000E-02   7.00000E+08
              1.25000E-01   8.02000E+08   1.00000E+00   8.02000E+08
     ASPECT
   3 NAME   "Steel plates"
     MCNAME MCSTEL
     MATMDL ISOTRO
     YOUNG    2.10000E+11
     POISON   3.00000E-01
     DENSIT   7.80000E+03
     ASPECT
   4 NAME   "Bond"
     USRIFC     BOTH

     DSNZ     1.3134E+13

     DSSY     1.3825E+12

     DSSX     1.3825E+12

     USRVAL        0     0.4     0.05     4.00E-03

                 0.00E+00     7.183E+07     1     4900000

                1.35E-04     7.183E+07     0.86     490

                2.80E-04     7.161E+07     0.78     0

                4.11E-04     7.126E+07     0.72     0

                                    Page 1
```

```
                                SP orginal
                6.21E-04     6.924E+07     0.65000     0

                8.30E-04     6.745E+07     0.59     0

                1.07E-03     6.249E+07     0.56     0

                1.51E-03     5.438E+07     0.52     0

                1.90E-03     5.057E+07     0.52     0

                2.60E-03     4.611E+07     0.52     0

                4.71E-03     3.886E+07     0.52     0

                1.21E-02     4.856E+06     0.52     0

                1.50E+20     0.000E+00     0.52     0

                 0 0

                 1E6 0.0

                 14E9 2.0            6.00E-03     0E-6 7.0

     USRSTA  0.0  0.0  0.0  0.0  0.0  0.0  0.0     1.31E+13     0.0 0.0 0.0 0.0
0.0

     USRIND  0 13 2
     ASPECT
   5 MCNAME INTERF
     MATMDL FRICTI
     IFTYP  SUR3D
     DSNZ     1.08000E+13
     DSSX     1.14000E+10
     DSSY     1.14000E+10
     FRICTI
     COHESI   1.00000E+00
     PHI      1.70000E-01
     PSI      1.70000E-01
     GAP
     MODE2  0
     GAPVAL   1.00000E+00
     ASPECT
'GEOMET'
   1 GCNAME SHEET
     GEOMDL STRINT
     XAXIS    0.00000E+00   1.00000E+00   0.00000E+00
   2 NAME   "Negative"
     GCNAME SHEET
     GEOMDL STRINT
     XAXIS    0.00000E+00  -1.00000E+00   0.00000E+00
   3 GCNAME SHEET
     GEOMDL STRINT
     XAXIS    0.00000E+00   5.00000E-01   0.00000E+00
   4 GCNAME SHEET
     GEOMDL STRINT
     XAXIS    0.00000E+00  -5.00000E-01   0.00000E+00
   5 GCNAME SHEET
     GEOMDL STRINT
     XAXIS    0.00000E+00  -5.00000E-01   0.00000E+00
   6 GCNAME SHEET
     GEOMDL STRINT
     XAXIS    0.00000E+00  -5.00000E-01   0.00000E+00
   7 GCNAME SHEET
     GEOMDL STRINT
     XAXIS    0.00000E+00   5.00000E-01   0.00000E+00
   8 GCNAME SHEET
     GEOMDL STRINT
```

```
                                    SP orginal
     XAXIS    0.00000E+00  -1.00000E+00   0.00000E+00
'ELEMENTS'
SET  "Beam"
CONNECT

MATERIAL 5
GEOMETRY 8
'LOADS'
CASE 1
NAME "Geometry load case 1"
WEIGHT
CASE 2
NAME "Geometry load case 2"
DEFORM
/ 25490 25493 25515-25526 / TR 3  -1.00000E-03
COMBIN
   1 1   1.00000E+00
   2 2   1.00000E+00
'SUPPOR'
NAME "Geometry support set 1"
/ 1 2 5 6 13 14 16 17 36 40-42 159-214 251-292 329-383 1021-1134 1617-2819
5649-5823 24908 24909 24935-24940 25036-25038 25083-25090 25199-25209 25363
25364 25397-25402 25492-25494 25539-25546 25656-25666 26367 26372-26374
26489-26602 26668-26729 / TR 2
/ 9 11 14-16 19 27-33 38-41 215-226 272-328 2820-3151 25828-25835 26308
26369-26373 26669 / TR 1
/ 25034 25037 25059-25070 / TR 3
NAME "Geometry support set 2"
/ 1 2 5 6 13 14 16 17 36 40-42 159-214 251-292 329-383 1021-1134 1617-2819
5649-5823 24908 24909 24935-24940 25036-25038 25083-25090 25199-25209 25363
25364 25397-25402 25492-25494 25539-25546 25656-25666 26367 26372-26374
26489-26602 26668-26729 / TR 2
/ 9 11 14-16 19 27-33 38-41 215-226 272-328 2820-3151 25828-25835 26308
26369-26373 26669 / TR 1
/ 25034 25037 25059-25070 25490 25493 25515-25526 / TR 3
'END'
```

```
: Diana Datafile written by Diana 10.1
'DIRECTIONS'
   1   1.00000E+00   0.00000E+00   0.00000E+00
   2   0.00000E+00   1.00000E+00   0.00000E+00
   3   0.00000E+00   0.00000E+00   1.00000E+00
'MODEL'
DIMENS "3D"
GRAVDI 3
GRAVAC  -9.81000E+00
'COORDINATES'

'MATERI'
   1 NAME   "Concrete"
     MCNAME CONCR
     MATMDL TSCR
     ASPECT
     POISON   2.00000E-01
     YOUNG    3.70000E+10
     DENSIT   2.40000E+03
     CBSPEC ROTS
     TOTCRK ROTATE
     TENCRV HORDYK
     GF1      1.51600E+02
     POIRED NONE
     TENSTR   4.10000E+06
     COMCRV THOREN
     CNFCRV VECCHI
     COMSTR   5.00000E+07
     LTHORE   3.00000E-01
     REDCRV NONE
   2 NAME   "Reinforcement steel"
     MCNAME MCSTEL
     MATMDL TRESCA
     ASPECT
     POISON   3.00000E-01
     YOUNG    2.22000E+11
     DENSIT   7.80000E+03
     TRESSH KAPSIG
     HARDEN STRAIN
     KAPSIG   0.00000E+00   7.00000E+08   7.00000E-02   7.00000E+08
              1.25000E-01   8.02000E+08   1.00000E+00   8.02000E+08
     YIELD  VMISES
   3 NAME   "Steel plates"
     MCNAME MCSTEL
     MATMDL ISOTRO
     ASPECT
     POISON   3.00000E-01
     YOUNG    2.10000E+11
     DENSIT   7.80000E+03
   4 NAME   "Bond"
     USRIFC     BOTH
     DSNZ     1.2303E+13
     DSSY     1.295E+12
     DSSX     1.295E+12
     USRVAL         0     0.4     0.05     4.00E-03
                 0.00E+00     5.000E+07     1     4100000
                1.35E-04     5.000E+07     0.86     410
                2.80E-04     4.985E+07     0.78     0
                4.11E-04     4.960E+07     0.72     0
                6.21E-04     4.820E+07     0.65000     0
                8.30E-04     4.695E+07     0.59     0
                1.07E-03     4.350E+07     0.56     0
                1.51E-03     3.785E+07     0.52     0
                1.90E-03     3.520E+07     0.52     0
                2.60E-03     3.210E+07     0.52     0
                4.71E-03     2.705E+07     0.52     0
                1.21E-02     3.380E+06     0.52     0
                1.50E+20     0.000E+00     0.52     0
```

```
                        SP50-GF208-fy700-corrosion-0
                0 0
                1E6 0.0
                14E9 2.0            6.00E-03     0E-6 7.0
     USRSTA  0.0  0.0  0.0  0.0  0.0  0.0  0.0     1.23E+13     0.0 0.0 0.0 0.0
0.0
     USRIND  0 13 2
   5 MCNAME INTERF
     MATMDL FRICTI
     ASPECT
     IFTYP  SUR3D
     DSNZ     1.08000E+13
     DSSX     1.14000E+10
     DSSY     1.14000E+10
     COHESI   1.00000E+00
     FRICTI
     GAP
     GAPVAL   1.00000E+00
     MODE2  0
     PHI      1.70000E-01
     PSI      1.70000E-01
'GEOMET'
   1 GCNAME SHEET
     GEOMDL STRINT
     XAXIS    0.00000E+00   1.00000E+00   0.00000E+00
   2 NAME   "Negative"
     GCNAME SHEET
     GEOMDL STRINT
     XAXIS    0.00000E+00  -1.00000E+00   0.00000E+00
   3 GCNAME SHEET
     GEOMDL STRINT
     XAXIS    0.00000E+00   5.00000E-01   0.00000E+00
   4 GCNAME SHEET
     GEOMDL STRINT
     XAXIS    0.00000E+00  -5.00000E-01   0.00000E+00
   5 GCNAME SHEET
     GEOMDL STRINT
     XAXIS    0.00000E+00  -5.00000E-01   0.00000E+00
   6 GCNAME SHEET
     GEOMDL STRINT
     XAXIS    0.00000E+00  -5.00000E-01   0.00000E+00
   7 GCNAME SHEET
     GEOMDL STRINT
     XAXIS    0.00000E+00   5.00000E-01   0.00000E+00
   8 GCNAME SHEET
     GEOMDL STRINT
     XAXIS    0.00000E+00  -1.00000E+00   0.00000E+00
'ELEMENTS'
SET  "Beam"
CONNECT

MATERIAL 5
GEOMETRY 8
'LOADS'
CASE 1
NAME "Geometry load case 1"
WEIGHT
CASE 2
NAME "Geometry load case 2"
DEFORM
/ 25490 25493 25515-25526 / TR 3  -1.00000E-03
COMBIN
   1 1   1.00000E+00
   2 2   1.00000E+00
'SUPPOR'
NAME "Geometry support set 1"
/ 1 2 5 6 13 14 16 17 36 40-42 159-214 251-292 329-383 1021-1134 1617-2819
5649-5823 24908 24909 24935-24940 25036-25038 25083-25090 25199-25209 25363
25364 25397-25402 25492-25494 25539-25546 25656-25666 26367 26372-26374
```

```
                          SP50-GF208-fy700-corrosion-0
26489-26602 26668-26729 / TR 2
/ 9 11 14-16 19 27-33 38-41 215-226 272-328 2820-3151 25828-25835 26308
26369-26373 26669 / TR 1
/ 25034 25037 25059-25070 / TR 3
NAME "Geometry support set 2"
/ 1 2 5 6 13 14 16 17 36 40-42 159-214 251-292 329-383 1021-1134 1617-2819
5649-5823 24908 24909 24935-24940 25036-25038 25083-25090 25199-25209 25363
25364 25397-25402 25492-25494 25539-25546 25656-25666 26367 26372-26374
26489-26602 26668-26729 / TR 2
/ 9 11 14-16 19 27-33 38-41 215-226 272-328 2820-3151 25828-25835 26308
26369-26373 26669 / TR 1
/ 25034 25037 25059-25070 25490 25493 25515-25526 / TR 3
'END'
```

```
                                    SP C30 (1)
: Diana Datafile written by Diana 10.1
'DIRECTIONS'
   1   1.00000E+00   0.00000E+00   0.00000E+00
   2   0.00000E+00   1.00000E+00   0.00000E+00
   3   0.00000E+00   0.00000E+00   1.00000E+00
'MODEL'
DIMENS "3D"
GRAVDI 3
GRAVAC  -9.81000E+00
'COORDINATES'

'MATERI'
   1 NAME   "Concrete"
     MCNAME CONCR
     MATMDL TSCR
     YOUNG    3.3000E+10
     POISON   2.00000E-01
     DENSIT   2.40000E+03
     TOTCRK ROTATE
     CBSPEC ROTS
     TENCRV HORDYK
     POIRED NONE
     TENSTR   2.90000E+06
     GF1      140.5
     COMCRV THOREN
     REDCRV NONE
     CNFCRV VECCHI
     COMSTR   3.00E+07
     LTHORE   3.00000E-01
     ASPECT
   2 NAME   "Reinforcement steel"
     MCNAME MCSTEL
     MATMDL TRESCA
     YOUNG    2.22000E+11
     POISON   3.00000E-01
     DENSIT   7.80000E+03
     YIELD  VMISES
     TRESSH KAPSIG
     HARDEN STRAIN
     KAPSIG   0.00000E+00   7.00000E+08   7.00000E-02   7.00000E+08
              1.25000E-01   8.02000E+08   1.00000E+00   8.02000E+08
     ASPECT
   3 NAME   "Steel plates"
     MCNAME MCSTEL
     MATMDL ISOTRO
     YOUNG    2.10000E+11
     POISON   3.00000E-01
     DENSIT   7.80000E+03
     ASPECT
   4 NAME   "Bond"
     USRIFC     BOTH

     DSNZ     1.0973E+13

     DSSY     1.155E+12

     DSSX     1.155E+12

     USRVAL        0     0.4     0.05     4.00E-03

                 0.00E+00     3.000E+07     1     2900000

                1.35E-04     3.000E+07     0.86     290

                2.80E-04     2.991E+07     0.78     0

                4.11E-04     2.976E+07     0.72     0
```

```
                                SP C30 (1)
                6.21E-04     2.892E+07     0.65000     0

                8.30E-04     2.817E+07     0.59     0

                1.07E-03     2.610E+07     0.56     0

                1.51E-03     2.271E+07     0.52     0

                1.90E-03     2.112E+07     0.52     0

                2.60E-03     1.926E+07     0.52     0

                4.71E-03     1.623E+07     0.52     0

                1.21E-02     2.028E+06     0.52     0

                1.50E+20     0.000E+00     0.52     0

                 0 0

                 1E6 0.0

                 14E9 2.0            6.00E-03     0E-6 7.0

     USRSTA  0.0  0.0  0.0  0.0  0.0  0.0  0.0     1.10E+13     0.0 0.0 0.0 0.0
0.0

     USRIND  0 13 2

     ASPECT
   5 MCNAME INTERF
     MATMDL FRICTI
     IFTYP  SUR3D
     DSNZ     1.08000E+13
     DSSX     1.14000E+10
     DSSY     1.14000E+10
     FRICTI
     COHESI   1.00000E+00
     PHI      1.70000E-01
     PSI      1.70000E-01
     GAP
     MODE2  0
     GAPVAL   1.00000E+00
     ASPECT
'GEOMET'
   1 GCNAME SHEET
     GEOMDL STRINT
     XAXIS    0.00000E+00   1.00000E+00   0.00000E+00
   2 NAME   "Negative"
     GCNAME SHEET
     GEOMDL STRINT
     XAXIS    0.00000E+00  -1.00000E+00   0.00000E+00
   3 GCNAME SHEET
     GEOMDL STRINT
     XAXIS    0.00000E+00   5.00000E-01   0.00000E+00
   4 GCNAME SHEET
     GEOMDL STRINT
     XAXIS    0.00000E+00  -5.00000E-01   0.00000E+00
   5 GCNAME SHEET
     GEOMDL STRINT
     XAXIS    0.00000E+00  -5.00000E-01   0.00000E+00
   6 GCNAME SHEET
     GEOMDL STRINT
     XAXIS    0.00000E+00  -5.00000E-01   0.00000E+00
   7 GCNAME SHEET
     GEOMDL STRINT
     XAXIS    0.00000E+00   5.00000E-01   0.00000E+00
   8 GCNAME SHEET
```

```
     GEOMDL STRINT
     XAXIS    0.00000E+00  -1.00000E+00   0.00000E+00
'ELEMENTS'
SET  "Beam"
CONNECT

MATERIAL 5
GEOMETRY 8
'LOADS'
CASE 1
NAME "Geometry load case 1"
WEIGHT
CASE 2
NAME "Geometry load case 2"
DEFORM
/ 25490 25493 25515-25526 / TR 3  -1.00000E-03
COMBIN
   1 1   1.00000E+00
   2 2   1.00000E+00
'SUPPOR'
NAME "Geometry support set 1"
/ 1 2 5 6 13 14 16 17 36 40-42 159-214 251-292 329-383 1021-1134 1617-2819
5649-5823 24908 24909 24935-24940 25036-25038 25083-25090 25199-25209 25363
25364 25397-25402 25492-25494 25539-25546 25656-25666 26367 26372-26374
26489-26602 26668-26729 / TR 2
/ 9 11 14-16 19 27-33 38-41 215-226 272-328 2820-3151 25828-25835 26308
26369-26373 26669 / TR 1
/ 25034 25037 25059-25070 / TR 3
NAME "Geometry support set 2"
/ 1 2 5 6 13 14 16 17 36 40-42 159-214 251-292 329-383 1021-1134 1617-2819
5649-5823 24908 24909 24935-24940 25036-25038 25083-25090 25199-25209 25363
25364 25397-25402 25492-25494 25539-25546 25656-25666 26367 26372-26374
26489-26602 26668-26729 / TR 2
/ 9 11 14-16 19 27-33 38-41 215-226 272-328 2820-3151 25828-25835 26308
26369-26373 26669 / TR 1
/ 25034 25037 25059-25070 25490 25493 25515-25526 / TR 3
'END'
```

```
: Diana Datafile written by Diana 10.1
'DIRECTIONS'
   1   1.00000E+00   0.00000E+00   0.00000E+00
   2   0.00000E+00   1.00000E+00   0.00000E+00
   3   0.00000E+00   0.00000E+00   1.00000E+00
'MODEL'
DIMENS "3D"
GRAVDI 3
GRAVAC  -9.81000E+00
'COORDINATES'

'MATERI'
   1 NAME   "Concrete"
     MCNAME CONCR
     MATMDL TSCR
     YOUNG    3.95000E+10
     POISON   2.00000E-01
     DENSIT   2.40000E+03
     TOTCRK ROTATE
     CBSPEC ROTS
     TENCRV HORDYK
     POIRED NONE
     TENSTR   4.90000E+06
     GF1      2.08700E+02
     COMCRV THOREN
     REDCRV NONE
     CNFCRV VECCHI
     COMSTR   7.18300E+07
     LTHORE   3.00000E-01
     ASPECT
   2 NAME   "Reinforcement steel"
     MCNAME MCSTEL
     MATMDL TRESCA
     YOUNG    2.22000E+11
     POISON   3.00000E-01
     DENSIT   7.80000E+03
     YIELD  VMISES
     TRESSH KAPSIG
     HARDEN STRAIN
     KAPSIG   0.00000E+00   7.00000E+08   7.00000E-02   7.00000E+08
              1.25000E-01   8.02000E+08   1.00000E+00   8.02000E+08
     ASPECT
   3 NAME   "Steel plates"
     MCNAME MCSTEL
     MATMDL ISOTRO
     YOUNG    2.10000E+11
     POISON   3.00000E-01
     DENSIT   7.80000E+03
     ASPECT
   4 NAME   "Bond"
     USRIFC     BOTH
     DSNZ     1.3134E+13
     DSSY     1.3825E+12
     DSSX     1.3825E+12
     USRVAL        0     0.4     0.05     4.00E-03
                 0.00E+00     7.183E+07     1     4900000
                1.35E-04     7.183E+07     0.86     490
                2.80E-04     7.161E+07     0.78     0
                4.11E-04     7.126E+07     0.72     0
                6.21E-04     6.924E+07     0.65000     0
                8.30E-04     6.745E+07     0.59     0
                1.07E-03     6.249E+07     0.56     0
                1.51E-03     5.438E+07     0.52     0
                1.90E-03     5.057E+07     0.52     0
                2.60E-03     4.611E+07     0.52     0
                4.71E-03     3.886E+07     0.52     0
                1.21E-02     4.856E+06     0.52     0
                1.50E+20     0.000E+00     0.52     0
```

```
                0 0
                1E6 1
                14E9 2.0            6.00E-03     0E-6 7.0
     USRSTA  0.0  0.0  0.0  0.0  0.0  0.0  0.0     1.31E+13     0.0 0.0 0.0 0.0
0.0
     USRIND  0 13 2
     ASPECT
   5 NAME   "Interface"
     MATMDL FRICTI
     ASPECT
     IFTYP  SUR3D
     DSNZ     1.08000E+13
     DSSX     1.14000E+10
     DSSY     1.14000E+10
     COHESI   1.00000E+00
     FRICTI
     GAP
     GAPVAL   1.00000E+00
     MODE2  0
     PHI      1.70000E-01
     PSI      1.70000E-01
'GEOMET'
   1 NAME   "Positive"
     GCNAME SHEET
     GEOMDL STRINT
     XAXIS    0.00000E+00   1.00000E+00   0.00000E+00
   2 NAME   "Negative"
     GCNAME SHEET
     GEOMDL STRINT
     XAXIS    0.00000E+00  -1.00000E+00   0.00000E+00
   3 GCNAME SHEET
     GEOMDL STRINT
     XAXIS    0.00000E+00   5.00000E-01   0.00000E+00
   4 GCNAME SHEET
     GEOMDL STRINT
     XAXIS    0.00000E+00  -5.00000E-01   0.00000E+00
'ELEMENTS'
SET  "Beam"
CONNECT

MATERIAL 4
GEOMETRY 4
'LOADS'
CASE 1
NAME "Geometry load case 1"
WEIGHT
CASE 2
NAME "Geometry load case 2"
DEFORM
/ 29479 29482 29504-29515 / TR 3  -1.00000E-03
'SUPPOR'
NAME "Geometry support set 1"
/ 1 2 5 6 13 14 16 17 36 40-42 167-230 267-308 345-408 1145-1276 1768-3148
6337-6541 28899 28900 28926-28931 29027-29029 29074-29081 29190-29200 29352
29353 29386-29391 29481-29483 29528-29535 29643-29653 30436 30441-30443
30576-30707 30782-30852 / TR 2
/ 9 11 14-16 19 27-33 38-41 231-242 288-344 3149-3480 29814-29821 30366
30438-30442 30783 / TR 1
/ 29025 29028 29050-29061 / TR 3
NAME "Geometry support set 2"
/ 1 2 5 6 13 14 16 17 36 40-42 167-230 267-308 345-408 1145-1276 1768-3148
6337-6541 28899 28900 28926-28931 29027-29029 29074-29081 29190-29200 29352
29353 29386-29391 29481-29483 29528-29535 29643-29653 30436 30441-30443
30576-30707 30782-30852 / TR 2
/ 9 11 14-16 19 27-33 38-41 231-242 288-344 3149-3480 29814-29821 30366
30438-30442 30783 / TR 1
/ 29025 29028 29050-29061 29479 29482 29504-29515 / TR 3
'END'
```

```
                                SPOrginalStirrups1
: Diana Datafile written by Diana 10.1
'DIRECTIONS'
   1   1.00000E+00   0.00000E+00   0.00000E+00
   2   0.00000E+00   1.00000E+00   0.00000E+00
   3   0.00000E+00   0.00000E+00   1.00000E+00
'MODEL'
DIMENS "3D"
GRAVDI 3
GRAVAC  -9.81000E+00
'COORDINATES'

'MATERI'
   1 NAME   "Concrete"
     MCNAME CONCR
     MATMDL TSCR
     YOUNG    3.95000E+10
     POISON   2.00000E-01
     DENSIT   2.40000E+03
     TOTCRK ROTATE
     CBSPEC ROTS
     TENCRV HORDYK
     POIRED NONE
     TENSTR   4.90000E+06
     GF1      2.08700E+02
     COMCRV THOREN
     REDCRV NONE
     CNFCRV VECCHI
     COMSTR   7.18300E+07
     LTHORE   3.00000E-01
     ASPECT
   2 NAME   "Reinforcement steel"
     MCNAME MCSTEL
     MATMDL TRESCA
     YOUNG    2.22000E+11
     POISON   3.00000E-01
     DENSIT   7.80000E+03
     YIELD  VMISES
     TRESSH KAPSIG
     HARDEN STRAIN
     KAPSIG   0.00000E+00   7.00000E+08   7.00000E-02   7.00000E+08
              1.25000E-01   8.02000E+08   1.00000E+00   8.02000E+08
     ASPECT
   3 NAME   "Steel plates"
     MCNAME MCSTEL
     MATMDL ISOTRO
     YOUNG    2.10000E+11
     POISON   3.00000E-01
     DENSIT   7.80000E+03
     ASPECT
   4 NAME   "Bond"
     USRIFC     BOTH

     DSNZ     1.3134E+13

     DSSY     1.3825E+12

     DSSX     1.3825E+12

     USRVAL        0     0.4     0.05     4.00E-03

                 0.00E+00     7.183E+07     1     4900000

                1.35E-04     7.183E+07     0.86     490

                2.80E-04     7.161E+07     0.78     0

                4.11E-04     7.126E+07     0.72     0

                                Page 1
```

```
                              SPOrginalStirrups1
                6.21E-04     6.924E+07     0.65000     0

                8.30E-04     6.745E+07     0.59     0

                1.07E-03     6.249E+07     0.56     0

                1.51E-03     5.438E+07     0.52     0

                1.90E-03     5.057E+07     0.52     0

                2.60E-03     4.611E+07     0.52     0

                4.71E-03     3.886E+07     0.52     0

                1.21E-02     4.856E+06     0.52     0

                1.50E+20     0.000E+00     0.52     0

                 0 0

                 1E6 0.0

                 14E9 2.0            6.00E-03     0E-6 7.0

     USRSTA  0.0  0.0  0.0  0.0  0.0  0.0  0.0     1.31E+13     0.0 0.0 0.0 0.0
0.0

     USRIND  0 13 2
     ASPECT
   5 MCNAME INTERF
     MATMDL FRICTI
     IFTYP  SUR3D
     DSNZ     1.08000E+13
     DSSX     1.14000E+10
     DSSY     1.14000E+10
     FRICTI
     COHESI   1.00000E+00
     PHI      1.70000E-01
     PSI      1.70000E-01
     GAP
     MODE2  0
     GAPVAL   1.00000E+00
     ASPECT
'GEOMET'
   1 GCNAME SHEET
     GEOMDL STRINT
     XAXIS    0.00000E+00   1.00000E+00   0.00000E+00
   2 NAME   "Negative"
     GCNAME SHEET
     GEOMDL STRINT
     XAXIS    0.00000E+00  -1.00000E+00   0.00000E+00
   3 GCNAME SHEET
     GEOMDL STRINT
     XAXIS    0.00000E+00   5.00000E-01   0.00000E+00
   4 GCNAME SHEET
     GEOMDL STRINT
     XAXIS    0.00000E+00  -5.00000E-01   0.00000E+00
   5 GCNAME SHEET
     GEOMDL STRINT
     XAXIS    0.00000E+00  -5.00000E-01   0.00000E+00
   6 GCNAME SHEET
     GEOMDL STRINT
     XAXIS    0.00000E+00  -5.00000E-01   0.00000E+00
   7 GCNAME SHEET
     GEOMDL STRINT
     XAXIS    0.00000E+00   5.00000E-01   0.00000E+00
   8 GCNAME SHEET
     GEOMDL STRINT
```

```
     XAXIS    0.00000E+00  -1.00000E+00   0.00000E+00
   9 NAME   "Stirrups"
     GCNAME RELINE
     GEOMDL REBAR
     CROSSE   2.82743E-05
'ELEMENTS'
SET  "Beam"
CONNECT

MATERIAL 5
GEOMETRY 8
'REINFORCEMENTS'
SET  "Stirrups"
LOCATI
   1 BAR

MATERIAL 2
GEOMETRY 9
SET  "Stirrups 1"
LOCATI
   2 BAR

MATERIAL 2
GEOMETRY 9
SET  "Stirrups 2"
LOCATI
   3 BAR

MATERIAL 2
GEOMETRY 9
SET  "Stirrups 3"
LOCATI
   4 BAR

MATERIAL 2
GEOMETRY 9
'LOADS'
CASE 1
NAME "Geometry load case 1"
WEIGHT
CASE 2
NAME "Geometry load case 2"
DEFORM
/ 25490 25493 25515-25526 / TR 3  -1.00000E-03
COMBIN
   1 1   1.00000E+00
   2 2   1.00000E+00
'SUPPOR'
NAME "Geometry support set 1"
/ 1 2 5 6 13 14 16 17 36 40-42 159-214 251-292 329-383 1021-1134 1617-2819
5649-5823 24908 24909 24935-24940 25036-25038 25083-25090 25199-25209 25363
25364 25397-25402 25492-25494 25539-25546 25656-25666 26367 26372-26374
26489-26602 26668-26729 / TR 2
/ 9 11 14-16 19 27-33 38-41 215-226 272-328 2820-3151 25828-25835 26308
26369-26373 26669 / TR 1
/ 25034 25037 25059-25070 / TR 3
NAME "Geometry support set 2"
/ 1 2 5 6 13 14 16 17 36 40-42 159-214 251-292 329-383 1021-1134 1617-2819
5649-5823 24908 24909 24935-24940 25036-25038 25083-25090 25199-25209 25363
25364 25397-25402 25492-25494 25539-25546 25656-25666 26367 26372-26374
26489-26602 26668-26729 / TR 2
/ 9 11 14-16 19 27-33 38-41 215-226 272-328 2820-3151 25828-25835 26308
26369-26373 26669 / TR 1
/ 25034 25037 25059-25070 25490 25493 25515-25526 / TR 3
'END'
```

```
                              Stallbacka 03-26 2.5MPa
: Diana Datafile written by Diana 10.1
'DIRECTIONS'
   1   1.00000E+00   0.00000E+00   0.00000E+00
   2   0.00000E+00   1.00000E+00   0.00000E+00
   3   0.00000E+00   0.00000E+00   1.00000E+00
'MODEL'
DIMENS "3D"
GRAVDI 3
GRAVAC  -9.81000E+00
'COORDINATES'

'MATERI'
   1 NAME   "Concrete"
     MCNAME CONCR
     MATMDL TSCR
     YOUNG    2.00000E+10
     POISON   2.00000E-01
     DENSIT   2.40000E+03
     TOTCRK ROTATE
     CBSPEC USER
     CRACKB   3.00000E-02
     TENCRV HORDYK
     POIRED DAMAGE
     TENSTR   2.50000E+06
     GF1      9.00264E+01
     COMCRV THOREN
     REDCRV VC1993
     REDMIN   0.00000E+00
     CNFCRV VECCHI
     COMSTR   4.80600E+07
     ASPECT
   2 NAME   "Steel"
     MCNAME STEEDC
     MATMDL EN1993
     STEEL  EN1993
     STANDA EN10025-3
     YOUNG    2.10000E+11
     POISON   3.00000E-01
     THERMX   1.20000E-05
     DENSIT   7.80000E+03
     GRADE  S275N
     NTHICK MAX40
     ASPECT
   4 NAME   "Bond"
     USRIFC     BOTH
     DSNZ     7.9800E+12
     DSSY     7E+11
     DSSX     7E+11
     USRVAL         0     0.4     0.05     4.00E-03
                 0.00E+00     4.806E+07     1     2500000
                 1.35E-04     4.806E+07     0.86     250
                 2.80E-04     4.792E+07     0.78     0
                 4.11E-04     4.768E+07     0.72     0
                 6.21E-04     4.633E+07     0.65000     0
                 8.30E-04     4.513E+07     0.59     0
                 1.07E-03     4.181E+07     0.56     0
                 1.51E-03     3.638E+07     0.52     0
                 1.90E-03     3.383E+07     0.52     0
                 2.60E-03     3.085E+07     0.52     0
                 4.71E-03     2.600E+07     0.52     0
                 1.21E-02     3.249E+06     0.52     0
                 1.50E+20     0.000E+00     0.52     0
                  0 0
                  1E6 0
                  14E9 2.0            8.00E-03     0E-6 7.0
     USRSTA  0.0  0.0  0.0  0.0  0.0  0.0  0.0     7.98E+12     0.0 0.0 0.0 0.0
0.0
     USRIND  0 13 2
```

```
      ASPECT
    5 NAME   "Reinforcement steel - stirrups/strength"
      MCNAME MCSTEL
      MATMDL ISOTRO
      YOUNG    2.06000E+11
      POISON   3.00000E-01
      DENSIT   7.80000E+03
      ASPECT
    3 NAME   "Reinforcement steel - main bars"
      MCNAME MCSTEL
      MATMDL TRESCA
      YOUNG    2.34000E+11
      POISON   3.00000E-01
      DENSIT   7.80000E+03
      YIELD  VMISES
      TRESSH NONE
      YLDSTR   6.00000E+02
      ASPECT
'GEOMET'
    1 NAME   "Stirrups"
      GCNAME RELINE
      GEOMDL REBAR
      CROSSE   2.82700E-05
    2 NAME   "S-bars"
      GCNAME RELINE
      GEOMDL REBAR
      CROSSE   3.14200E-04
    3 NAME   "Bond 1"
      GCNAME SHEET
      GEOMDL PLSTRA
      XAXIS   -1.00000E+00   0.00000E+00   0.00000E+00
    4 NAME   "Bond 2"
      GCNAME SHEET
      GEOMDL PLSTRA
      XAXIS   -1.00000E+00   0.00000E+00   0.00000E+00
    5 NAME   "Bond 3"
      GCNAME SHEET
      GEOMDL PLSTRA
      XAXIS    1.00000E+00   0.00000E+00   0.00000E+00
    6 NAME   "Bond 4"
      GCNAME SHEET
      GEOMDL PLSTRA
      XAXIS    1.00000E+00   0.00000E+00   0.00000E+00
    7 NAME   "Bond 5"
      GCNAME SHEET
      GEOMDL PLSTRA
      XAXIS    1.00000E+00   0.00000E+00   0.00000E+00
    8 NAME   "Bond 6"
      GCNAME SHEET
      GEOMDL PLSTRA
      XAXIS    1.00000E+00   0.00000E+00   0.00000E+00
    9 NAME   "Bond 7"
      GCNAME SHEET
      GEOMDL PLSTRA
      XAXIS   -1.00000E+00   0.00000E+00   0.00000E+00
   10 NAME   "Bond 8"
      GCNAME SHEET
      GEOMDL PLSTRA
      XAXIS   -1.00000E+00   0.00000E+00   0.00000E+00
'ELEMENTS'
SET  "Beam"
CONNECT

MATERIAL 4
GEOMETRY 10
'REINFORCEMENTS'
SET  "Stirrup 1"
LOCATI
```

```
   1 BAR

MATERIAL 5
GEOMETRY 1
SET  "S-bar 3"
LOCATI
   2 BAR

MATERIAL 5
GEOMETRY 2
SET  "S-bar 1"
LOCATI
   3 BAR

MATERIAL 5
GEOMETRY 2
SET  "S-bar 2"
LOCATI
   4 BAR

MATERIAL 5
GEOMETRY 2
SET  "S-bar 4"
LOCATI
   5 BAR

MATERIAL 5
GEOMETRY 2
SET  "Stirrup 2"
LOCATI
   6 BAR

MATERIAL 5
GEOMETRY 1
SET  "Stirrup 3"
LOCATI
   7 BAR

MATERIAL 5
GEOMETRY 1
SET  "Stirrup 4"
LOCATI
   8 BAR

MATERIAL 5
GEOMETRY 1
'LOADS'
CASE 1
NAME "Geometry load case 1"
WEIGHT
CASE 2
NAME "Geometry load case 2"
DEFORM
/ 26326-26353 26358-26388 / TR 3  -1.00000E-03
COMBIN
   1 1   1.00000E+00
   2 2   1.00000E+00
   3 2   1.00000E+00
'SUPPOR'
NAME "Support set 1"
/ 7 10-12 18-21 23 25 33-39 47-53 61-67 75-81 89-95 97 98 101 104 112-118
126-132 319-331 345-371 386-397 3245-5194 26471-26478 26855 26913-26920 27297
27348-27355 27732 27783-27790 28167 28216-28223 28600 28651-28658 29035
29087-29094 29471 / TR 2
/ 6 133-136 140-143 146 3110-3174 8996-9010 / TR 1
/ 6 133-136 140-143 146 3110-3174 8996-9010 26326-26353 26358-26388 / TR 3
'END'
```